JACS
JOURNAL OF THE AMERICAN CHEMICAL SOCIETY
pubs.acs.org/JACS
Article

Controlling Intramolecular and Intermolecular Electronic Coupling of Radical Ligands in a Series of Cobaltoviologen Complexes

Brice J. O. Kessler, Iram F. Mansoor, Derek I. Wozniak, Thomas J. Emge, and Mark C. Lipke*

Cite This: J. Am. Chem. Soc. 2023, 145, 15924−15935
Read Online
ACCESS | Metrics & More | Article Recommendations | Supporting Information

ABSTRACT: Controlling electronic coupling between multiple redox sites is of interest for tuning the electronic properties of molecules and materials. While classic mixed-valence (MV) systems are highly tunable, e.g., via the organic bridges connecting the redox sites, metal-bridged MV systems are difficult to control because the electronics of the metal cannot usually be altered independently of redox-active moieties embedded in its ligands. Herein, this limitation was overcome by varying the donor strengths of ancillary ligands in a series of cobalt complexes without directly perturbing the electronics of viologen-like redox sites bridged by the cobalt ions. The cobaltoviologens $[\mathbf{1_X\text{-}Co}]^{n+}$ feature four 4-X-pyridyl donor groups (X = CO_2Me, Cl, H, Me, OMe, NMe_2) that provide gradual electronic tuning of the bridging Co^{II} centers, while a related complex $[\mathbf{2\text{-}Co}]^{n+}$ with NHC donors supports exclusively Co^{III} states even upon reduction of the viologen units. Electrochemistry and IVCT band analysis indicate that the MV states of these complexes have electronic structures ranging from fully localized ($[\mathbf{2\text{-}Co}]^{4+}$; Robin−Day Class I) to fully delocalized ($[\mathbf{1_{CO2Me}\text{-}Co}]^{3+}$; Class III) descriptions, demonstrating unprecedented control over electronic coupling without changing the identity of the redox sites or bridging metal. Additionally, single-crystal XRD characterization of the homovalent complexes $[\mathbf{1_H\text{-}Co}]^{2+}$ and $[\mathbf{1_H\text{-}Zn}]^{2+}$ revealed radical-pairing interactions between the viologen ligands of adjacent complexes, representing a type of through-space electronic coupling commonly observed for organic viologen radicals but never before seen in metalloviologens. The extended solid-state packing of these complexes produces 3D networks of radical π-stacking interactions that impart unexpected mechanical flexibility to these crystals.

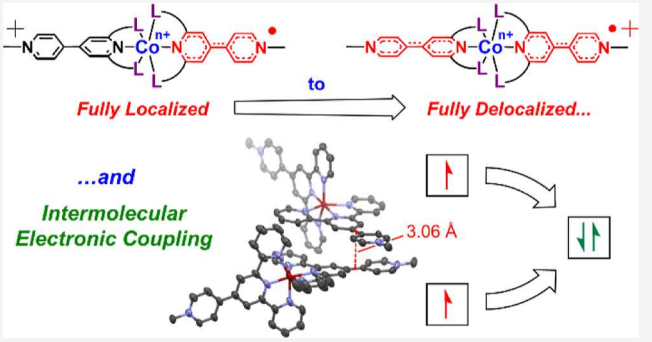

INTRODUCTION

Mixed-valence (MV) systems that show electronic coupling between their redox sites are of longstanding interest[1,2] for their nuanced electronic structures,[3] which lie on a continuum from fully localized[2a,b] to fully delocalized[2f,g] descriptions (Scheme 1A). The strength of coupling can influence electron-transfer processes,[4] conductivity,[5] and other chemical or physical properties[6] of molecules and materials, thus motivating considerable interest in controlling coupling between redox sites.[7−17] Classic MV examples, with two redox-active metals connected by a conjugated bridge (Scheme 1B),[2e] have been tuned by changing the metal centers,[7] the bridge,[8] or the ancillary ligands.[9] Likewise, organic MV systems are often highly tunable owing to the synthetic versatility of organic chemistry.[10−12] These examples reveal how electronic coupling is influenced by factors such as the length and conjugation pathway of the bridge,[11] as well as its orbital energies relative to those of the redox sites.[10b,12] However, there remain substantial limitations to the control that can be attained over electronic delocalization in many MV systems, especially those in which two organic redox sites are coupled by a bridging metal ion.[13]

Most metal-bridged MV systems, including complexes of salen,[2g,14] diarylamido,[15] pyridine-diimine (PDI),[16] and dithiolene ligands (Scheme 2A),[17,18] exhibit ligand-based redox activity that heavily involves donor atoms bound to the bridging metal,[19] making it challenging to independently tune the properties of the redox sites and the bridge. Thus, while reduction potentials of such complexes can be altered by > 500 mV using electron-donating (ED) and -withdrawing (EW) substituents, these changes weakly influence the electronic coupling of the ligands.[14a,b,15b,16a] Recently reported aluminum bis-PDI complexes exhibit reduction potentials spanning a 0.5 V range while maintaining Robin−Day Class III (fully delocalized) or borderline Class II/III (nearly fully delocalized) descriptions.[16a] A greater variation in coupling, from Class II (moderately coupled) to Class III, was seen in a

Received: April 11, 2023
Published: July 17, 2023

https://doi.org/10.1021/jacs.3c03725
J. Am. Chem. Soc. 2023, 145, 15924−15935

Scheme 1. Electronically Coupled Redox Systems

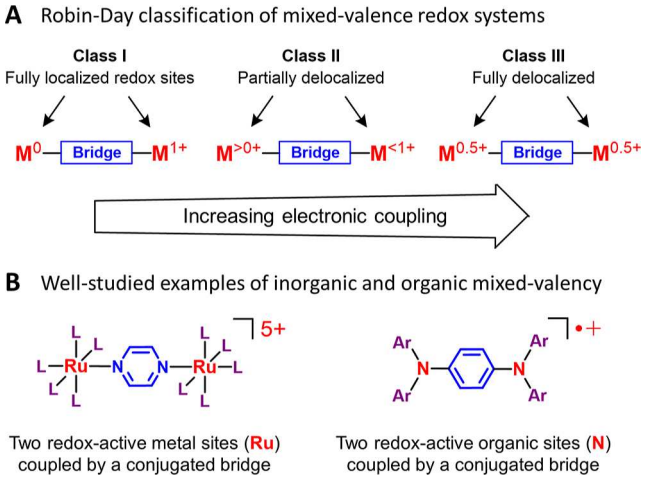

series of nickel-salen complexes, but required a 0.77 V variation in the reduction potentials of the ligands.[14a,b] On the other extreme, changing the bridging metal often disrupts delocalization considerably,[6a,13c,14d,15a] providing only a crude tool for tuning such systems. Identifying more precisely tunable metal-bridged MV systems would fill an important gap in the study of mixed valency and may also lead to practical advances since delocalized complexes can serve as important components of electronic materials (e.g., conductive[5d,e] and electrocatalytic[20] MOFs).

We recently discovered that cobalt mediates borderline Class II/III electronic coupling between viologen-like redox sites embedded in simple terpyridine ligand scaffolds (complex $[\mathbf{1_H}\text{-}\mathbf{Co}]^{3+}$ in Scheme 2B).[6a] Since redox activity is centered almost entirely on the viologen cores, we hypothesized that the flanking donor groups of the ligands could be altered to modulate the electronics of the cobalt bridge while minimally perturbing the organic redox sites (Scheme 2B), thereby affording substantial control over the ability of cobalt to mediate coupling between these sites. Herein, we describe the success of this strategy at gradually tuning the MV states of the cobaltoviologens from Class I to Class III descriptions, representing a range of variation and degree of control unavailable in any other series of metal-bridged MV systems that maintain a fixed set of redox sites and bridging metal. Even among organic-bridged MV systems, it is rare to achieve high tunability in isostructural examples[10b] since the bridge length and geometry are often major factors in determining the strength of coupling.[2c,3d,8,10a,11]

The electronic tunability, long path of delocalization (up to ~1.8 nm), and structural invariance of the cobaltoviologens may make these complexes useful for developing new electronic materials, especially considering that simpler viologens are already of substantial interest in this regard.[21−23] Thus, it is also notable that the more reduced complex $[\mathbf{1_H}\text{-}\mathbf{Co}]^{2+}$ and its zinc analogue $[\mathbf{1_H}\text{-}\mathbf{Zn}]^{2+}$ were found to engage in π-radical-pairing interactions that represent a type of through-space electronic coupling characteristic of organic viologens[21] but which has not been observed before in metalloviologens or any other heteroatom-substituted viologen derivatives.[22] Such interactions contribute to the conductivity of viologen-radical crystals and have been used to prepare nanomaterials with a variety of unique electronic and mechanical properties.[23] The ability of metalloviologens to participate in these interactions further suggests that these complexes may provide a rich basis for developing new materials. Underscoring this possibility, $[\mathbf{1_H}\text{-}\mathbf{Co}]^{2+}$ and $[\mathbf{1_H}\text{-}\mathbf{Zn}]^{2+}$ pack into crystalline 3D networks in which the combination of metal−ligand coordination and radical π-stacking gives rise to emergent mechanical flexibility not observed in organic viologen crystals.

RESULTS AND DISCUSSION

Design and Synthesis of New Cobaltoviologens. The complex $[\mathbf{1_H}\text{-}\mathbf{Co}]^{4+}$ was first reported over 20 years ago,[24] but we only recently discovered that its reduced state $[\mathbf{1_H}\text{-}\mathbf{Co}]^{3+}$ exhibits a delocalized electronic structure,[6a] in contrast to its Fe^{II}, Ni^{II}, and Zn^{II} analogues, which undergo localized ligand reductions.[6a,25] A half-filled 3d orbital of d_{xz}/d_{yz} parentage appears to be important for the delocalized electronic structure of the cobalt derivative;[6a] therefore, tuning the energy and occupancy of this orbital was targeted to control its ability to facilitate inter-ligand electronic coupling. The Co^{II}/Co^{I} reduction potentials of simple $[(terpy)_2Co]^{2+}$ complexes can be modified across a wide range using electron-donating or -withdrawing substituents on the flanking pyridyl groups,[26a] suggesting an easy way to tune the electronics of the cobalt bridge in $[\mathbf{1_X}\text{-}\mathbf{Co}]^{n+}$. Additionally, it was envisioned that strong donor groups might even lead to changes in the spin state or oxidation state of the cobalt center, which would offer a novel way to control electronic coupling between the ligands in these complexes.[27]

A series of new terpy-viologen ligands $\mathbf{1_X}^+$ was prepared with 4-position substituents (X = CO_2Me, Cl, Me, OMe, and NMe_2) on the flanking pyridyl groups that provide a well-spaced gradient from strongly electron withdrawing to strongly electron donating (Scheme 3). In all cases, the new ligands were prepared from 4-substituted 2-acetylpyridines using the

Scheme 2. Tuning Metal-Mediated Electronic Coupling of Organic Redox Sites

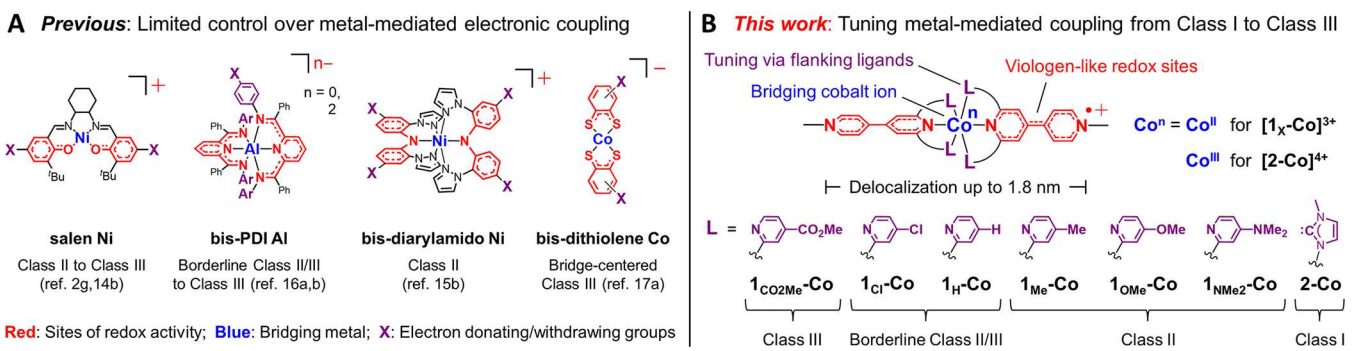

https://doi.org/10.1021/jacs.3c03725
J. Am. Chem. Soc. 2023, 145, 15924−15935

Scheme 3. Synthesis of $[\mathbf{1_X}\text{-Co}]\cdot n\mathrm{PF_6}$ and $[\mathbf{1_X}\text{-Zn}]\cdot 4\mathrm{PF_6}$

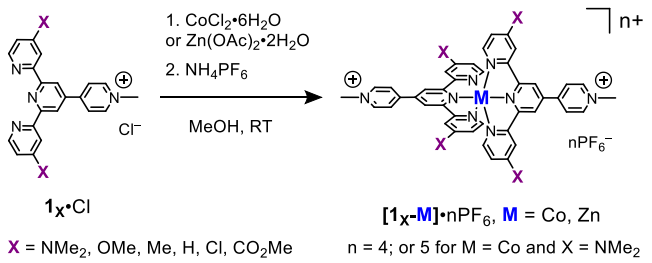

established terpyridine synthesis and *N*-methylation sequence used to prepare $\mathbf{1_H}^+$ (see the Supporting Information for synthetic details).[28,29] Once the ligands $\mathbf{1_X}^+$ were isolated as chloride salts, they readily formed the bis-terpy complexes $[\mathbf{1_X}\text{-Co}]^{4+}$ and $[\mathbf{1_X}\text{-Zn}]^{4+}$ upon treatment with $CoCl_2\cdot 6H_2O$ or $Zn(OAc)_2\cdot 2H_2O$. Paramagnetic ^{1}H NMR spectra (Figures S36−S40), Evans method magnetic measurements (Table S1), and UV−vis spectra (Figures S77, S81, S85, S89, and S94) indicate that the $[\mathbf{1_X}\text{-Co}]^{4+}$ complexes all have similar electronic structures with low-spin and high-spin Co^{II} in equilibrium at 25 °C. However, the NMe_2-substituted derivative oxidizes to a Co^{III} state under air, so samples were isolated in this higher oxidation state ($[\mathbf{1_{NMe2}}\text{-Co}]^{5+}$) for ease of handling (see Figure S19 for diamagnetic ^{1}H NMR spectrum).

To access more dramatic electronic changes in the cobaltoviologens, a bis-NHC-viologen pincer ligand $\mathbf{2}^+$ was designed to provide highly donating flanking groups.[26b] The NHC ligand precursor $\mathbf{2\text{-}H}^{3+}$ was prepared readily (Scheme 4)

Scheme 4. Synthesis of $[\mathbf{2}\text{-Co}]\cdot 5\mathrm{PF_6}$

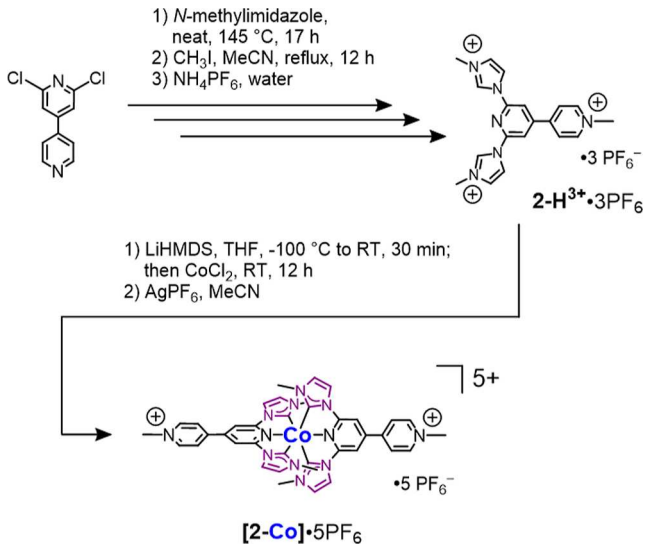

by nucleophilic aromatic substitution of 2,6-dichloro-4,4′-bipyridine with *N*-methylimidazole, followed by methylation of the 4-pyridyl group. Metallation of $\mathbf{2\text{-}H}^{3+}$ with cobalt was achieved by deprotonating the ligand precursor with LiHMDS at −100 °C in THF, followed by treatment with $CoCl_2$, and lastly, oxidation with $AgPF_6$ to provide the Co^{III} complex $[\mathbf{2}\text{-Co}]^{5+}$ (Scheme 4). Though less straightforward than the preparation of the $[\mathbf{1_X}\text{-Co}]^{n+}$ complexes, $[\mathbf{2}\text{-Co}]^{5+}$ was successfully isolated and characterized by ^{1}H NMR spectroscopy and ESI-HRMS (Figures S34, S35, S59).

Electrochemical Characterization. Cyclic voltammetry was used to examine the redox properties of the new metalloviologens, revealing how the flanking donor groups affect reduction potentials of the viologen units and the extent to which these redox processes are influenced by inter-ligand electronic coupling. None of the zinc complexes show separation of the first reductions of each ligand (Figures 1 and S69−S73), consistent with a lack of electronic communication through the Zn^{II} bridge. The $E_{1/2}$ values (−0.95 to −1.12 V vs $Fc^{+/0}$) for these ligand-centered 2 e^- redox processes vary with the electron-donating/withdrawing character of the substituents on the ligands, showing a good linear correlation with their σ_p Hammett parameters but not with the corresponding σ_m values (Figure S74). Since the substituents on the flanking groups are in the meta position relative to the viologen moieties, the correlation of $E_{1/2}$ with σ_p but not σ_m suggests that the flanking pyridyl groups influence the redox properties of the viologens by tuning the Lewis acidity of the Zn^{II} ion rather than via direct inductive effects. Two closely overlapping 1 e^- reductions follow the 2 e^- first reduction, and the consistently small spacing (68−81 mV) between these 1 e^- reductions confirms the absence of significant electronic communication between the ligands in any of the redox states of $[\mathbf{1_X}\text{-Zn}]^{n+}$.

The $[\mathbf{1_X}\text{-Co}]^{n+}$ series exhibits redox behavior differing significantly from that of their zinc counterparts. The cobalt complexes all show four distinct 1 e^- redox couples involving the viologen units (Figure 1 and Table 1), with the separation between the first and second of these reductions changing from $\Delta E_{red1,2}$ = 122 mV to $\Delta E_{red1,2}$ = 396 mV ($\Delta\Delta E_{red1,2}$ = 274 mV) across the series from $[\mathbf{1_{NMe2}}\text{-Co}]^{n+}$ to $[\mathbf{1_{CO2Me}}\text{-Co}]^{n+}$. The increasing separation corresponds to increasing electronic coupling between the ligands in the 3+ state,[30] confirming that the flanking donor groups are effective for tuning delocalization across the L-Co-L core, while paramagnetic ^{1}H NMR shifts indicate that $[\mathbf{1_{NMe2}}\text{-Co}]^{3+}$ and $[\mathbf{1_{CO2Me}}\text{-Co}]^{3+}$ otherwise have electronic structures resembling that of $[\mathbf{1_H}\text{-Co}]^{3+}$ in which the viologen π^* radical couples antiferromagnetically to h.s. Co^{II} (Figures S41 and S42). Interestingly, the midpoint between the first and second reductions ($E_{mid1,2}$), which approximates what the potential of the ligand-based reductions would be in the absence of coupling, changes by only 237 mV across this series (see Table 1). This observation confirms that the electronics of the $\mathbf{1_X}$-Co complexes are influenced more by variation in electronic coupling between the ligands than by variation of the individual properties of each ligand. Likewise, though a good correlation was seen between σ_p and $E_{mid1,2}$ (Figure S65), an even better correlation was seen between σ_p and the comproportionation constants (log K_c) for the $[\mathbf{1_X}\text{-Co}]^{4+}$ and $[\mathbf{1_X}\text{-Co}]^{2+}$ states (Figure 2). Since the K_c values are proportional to the strength of coupling between the viologens, this latter observation confirms that control over delocalization is determined by the donor strength of the flanking pyridines.

The third and fourth ligand-centered reductions of $[\mathbf{1_X}\text{-Co}]^{n+}$ also show substantial separation for each derivative, spanning from $\Delta E_{red3,4}$ = 242 mV for $[\mathbf{1_{NMe2}}\text{-Co}]^{n+}$ to $\Delta E_{red3,4}$ = 308 mV for $[\mathbf{1_{CO2Me}}\text{-Co}]^{n+}$. The large $\Delta E_{red3,4}$ value for the NMe_2 derivative suggests much stronger inter-ligand electronic coupling in the 1+ mixed-valence state of this complex than in its 3+ state, consistent with the behavior of the few other known metal-bridged systems that show multiple MV states.[16a,b,31] However, $\Delta E_{red3,4}$ increases only gradually across the $[\mathbf{1_X}\text{-Co}]^{1+}$ series, and it is unclear why electronic coupling

https://doi.org/10.1021/jacs.3c03725
J. Am. Chem. Soc. 2023, 145, 15924−15935

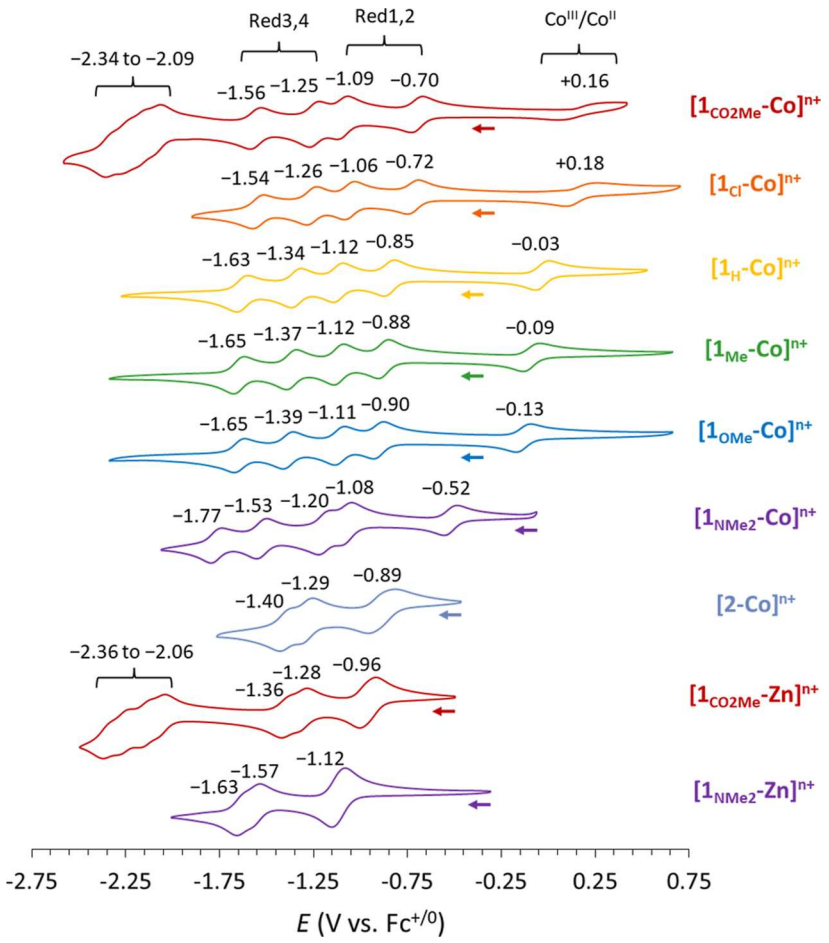

Figure 1. Cyclic voltammograms of $[\mathbf{1_X\text{-}Co}](PF_6)_n$, $[\mathbf{2\text{-}Co}](PF_6)_5$, and select $[\mathbf{1_X\text{-}Zn}](PF_6)_4$ complexes in MeCN containing 0.1 M $TBAPF_6$ at a scan rate of 0.1 V s^{-1}. The $E_{1/2}$ values of each redox couple are indicated to the nearest 10 mV, except for reductions of the flanking pyridyl groups of the $[\mathbf{1_{CO2Me}\text{-}M}]^{n+}$ derivatives, for which ranges are given from the most negative to the most positive $E_{1/2}$ values of these overlapping couples.

Table 1. Analysis of CV Data for Complexes $[\mathbf{1_X\text{-}Co}]^{n+}$

X	$E_{mid1,2}$[a] (V vs Fc+/0)	$\Delta E_{red1,2}$ (mV)	$E_{mid3,4}$[a] (V vs Fc$^{+/0}$)	$\Delta E_{red3,4}$ (mV)
CO_2Me	−0.90	396	−1.41	308
Cl	−0.89	338	−1.40	284
H	−0.98[b]	272[b]	−1.49[b]	288[b]
Me	−1.00	237	−1.51	280
OMe	−1.01	207	−1.52	260
NMe_2	−1.14	122	−1.65	242

[a]Midpoint value between the first and second reduction potentials (red1,2) or third and fourth reduction potentials (red3,4) listed to the nearest 10 mV. [b]Data from ref 6a.

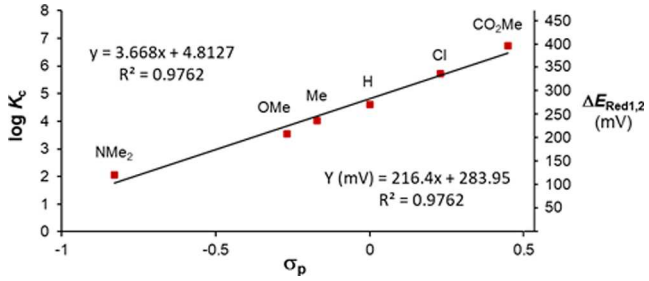

Figure 2. Correlation of the comproportionation constants (log K_c) for the n = 4+ and 2+ states of $[\mathbf{1_X\text{-}Co}]^{n+}$ with the σ_p Hammett parameter of the substituents on the flanking pyridyl groups of the ligands. $\Delta E_{red1,2}$ values are labeled on the right-hand axis.

would be less responsive to tuning in the 1+ states than in the 3+ states. We speculate that other factors (e.g., degree of metal-centered reduction; structural changes that viologens undergo in their most reduced states[32,33]) might also influence $\Delta E_{red3,4}$, preventing a reliable interpretation of these values.

The redox properties of NHC-based $[(CNC)_2Co]^{3+}$ complexes are not well established,[26b] making it difficult to predict how the NHC donors in $[\mathbf{2\text{-}Co}]^{5+}$ would influence the reduced states of this complex. Interestingly, $[\mathbf{2\text{-}Co}]^{5+}$ exhibits CVs that are more like those of the $[\mathbf{1_X\text{-}Zn}]^{4+}$ complexes than those of the other cobaltoviologens. The first reduction of $[\mathbf{2\text{-}Co}]^{5+}$ is a ligand-centered quasireversible 2 e^- process occurring at $E_{1/2}$ = −0.885 V (Figure 1) with a minimum peak separation of ∼130 mV (Figure S75), which is slightly wider than that (∼80 mV) observed for the 2 e^- first reduction of the zinc complexes. Likewise, subsequent 1 e^- reductions of $[\mathbf{2\text{-}Co}]^{n+}$ ($E_{1/2}$ = −1.28, −1.40 V, ΔE = 120 mV) are spaced slightly wider than for the zinc complexes but still much narrower than for the corresponding reductions of the $[\mathbf{1_X\text{-}Co}]^{n+}$ series. These data reveal that $[\mathbf{2\text{-}Co}]^{n+}$ exhibits much weaker inter-ligand electronic coupling than that observed for the terpy-based cobaltoviologens.

The weaker electronic coupling in $[\mathbf{2\text{-}Co}]^{n+}$ versus $[\mathbf{1_X\text{-}Co}]^{n+}$ likely arises from the different oxidation states of cobalt in these complexes. The NHC-supported complex does not

https://doi.org/10.1021/jacs.3c03725
J. Am. Chem. Soc. 2023, 145, 15924−15935

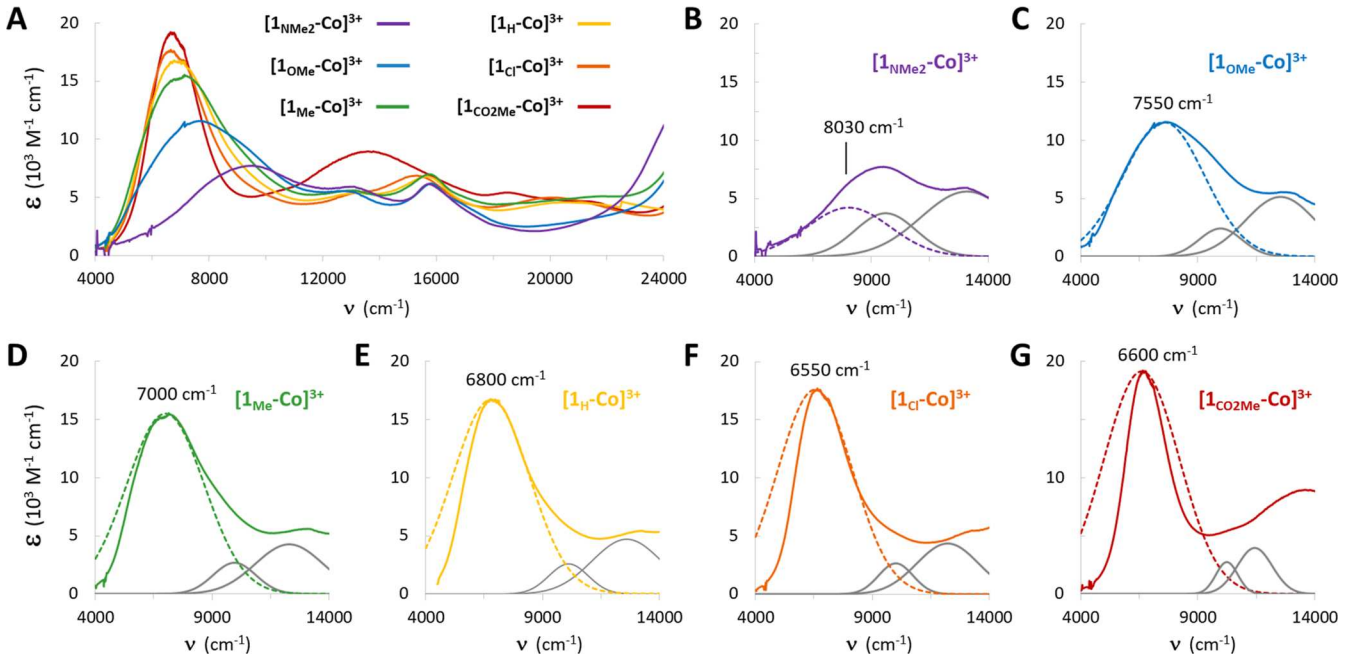

Figure 3. NIR-vis regions of the spectra of $[\mathbf{1_X\text{-}Co}]^{3+}$. (A) Overlay of all spectra in this series. (B–G) IVCT analysis of each spectrum from that of (B) $[\mathbf{1_{NMe2}\text{-}Co}]^{3+}$ to (G) $[\mathbf{1_{CO2Me}\text{-}Co}]^{3+}$. Solid colored lines show the experimental spectra, dotted colored lines depict theoretical Gaussian IVCT bands with their ε_{max} values indicated, and gray lines depict two freely refined Gaussian bands that overlap partially with the IVCT bands (see Figures S102–S107 for full Gaussian deconvolution of the NIR-vis regions of these spectra).

exhibit a Co^{III}/Co^{II} reduction prior to reduction of its ligands (Figure S76), and thus, the reduced viologen units are bridged by Co^{III} instead of the Co^{II} centers in $[\mathbf{1_X\text{-}Co}]^{n+}$. Since Co^{III} is low spin, the π-symmetry 3d orbitals[34] of $[\mathbf{2\text{-}Co}]^{n+}$ are fully occupied and unavailable for communicating an electron between the ligands. These results provide valuable experimental validation of past DFT calculations (which are often unreliable for MV systems[3b,35]) indicating that coupling in $[\mathbf{1_H\text{-}Co}]^{3+}$ is facilitated by a half-filled 3d orbital that interacts with both viologen π-systems.[6a] Notably, the ability to control the oxidation and spin state of cobalt in the cobaltoviologens is a unique feature of these MV systems, representing a novel way to tune electronic coupling.[27]

Returning to the $[\mathbf{1_x\text{-}Co}]^{n+}$ series, the CO_2Me derivative shows four additional overlapping redox processes negative of −2.0 V vs $Fc^{+/0}$ that provide additional confirmation of the role of orbital occupancy in promoting delocalization. These redox features, which are also seen for the zinc derivative, can be attributed to reduction of the four electron-deficient flanking pyridyl groups and do not exhibit substantial separation for either the cobalt or zinc complexes. Thus, while the cobalt center in $[\mathbf{1_{CO2Me}\text{-}Co}]^{n+}$ is able to electronically couple the viologen moieties, it does not show this effect for the flanking pyridyl groups. Since Co^{II} can have only one of its π-symmetry d-orbitals partially occupied, and this orbital couples the viologens,[6a] there is no d-orbital available for coupling the flanking pyridyl groups.

Classifying Electronic Coupling by IVCT Band Analysis. The comproportionation constants (log K_c = 2.07 to 6.71) for the n = 4+ and 2+ states of the $[\mathbf{1_X\text{-}Co}]^{n+}$ series suggest that there is considerable variation in the electronic coupling between the ligands in the 3+ states of these complexes. However, since K_c values can be unreliable for classifying electronic delocalization,[36] UV–vis–NIR spectroscopy was employed for a clearer analysis. All the $[\mathbf{1_X\text{-}Co}]^{3+}$ complexes exhibit a well-defined near-IR intervalence charge-transfer (IVCT) band[3] (Figure 3), which increases in intensity and decreases in width with increasing EW character of the flanking donor groups of the ligands, consistent with increasing electronic coupling between the redox-active units of the ligands.[3]

The IVCT bands were analyzed to assign Robin–Day classifications to each $[\mathbf{1_X\text{-}Co}]^{3+}$ complex. We previously classified $[\mathbf{1_H\text{-}Co}]^{3+}$ by fitting its IVCT band to a Gaussian curve in order to extract the full-width at half maximum ($\Delta\nu_{1/2}$) of the band and the electronic coupling parameter (H_{ab}),[6a] both of which indicate the strength of electronic coupling.[3] Although this approach is commonly used to analyze mixed-valence systems,[10c,11a,16a,b] it suffers from two major limitations: (1) strongly coupled systems lead to truncation of the IVCT band on its low energy side, so it does not maintain a Gaussian shape; and (2) calculating H_{ab} requires the distance (r_{ab}) between the redox sites,[3] which is not well defined in $[\mathbf{1_X\text{-}Co}]^{3+}$ since each viologen unit is itself a delocalized π-system. Thus, we employed a more sophisticated method of IVCT analysis for comparing electronic coupling in the $[\mathbf{1_X\text{-}Co}]^{3+}$ series of complexes.[3a,11d] The ν_{max} values of the observed IVCT bands were used to calculate theoretical Gaussian IVCT bands assuming Class II coupling,[3a] and these theoretical bands were combined with four to five freely refined Gaussian curves to fit the vis-NIR region of each spectrum (see Figures S102–S107), confirming that features aside from the IVCT bands are relatively consistent. Robin–Day classifications were then assigned by comparing the theoretical and experimental IVCT bands to measure truncation of the latter (Figure 3B–G), which is directly related to the strength of electronic coupling between the ligands.

As can be seen in Figure 3B,C, the most electron-rich complexes $[\mathbf{1_{NMe2}\text{-}Co}]^{3+}$ and $[\mathbf{1_{OMe}\text{-}Co}]^{3+}$ have IVCT bands

https://doi.org/10.1021/jacs.3c03725
J. Am. Chem. Soc. 2023, 145, 15924–15935

that are well matched to theoretical Gaussian curves even on the low-energy sides of these absorptions, consistent with Class IIA coupling,[3a] though the high intensity and slight truncation of the IVCT band for $[\mathbf{1}_{\mathbf{OMe}}\text{-}\mathbf{Co}]^{3+}$ suggests that this complex is at the upper limit of this assignment. The complexes $[\mathbf{1}_{\mathbf{Me}}\text{-}\mathbf{Co}]^{3+}$, $[\mathbf{1}_{\mathbf{H}}\text{-}\mathbf{Co}]^{3+}$, and $[\mathbf{1}_{\mathbf{Cl}}\text{-}\mathbf{Co}]^{3+}$ show more noticeable truncation on the low-energy side of their IVCT bands (Figure 3D−F), which increases as the donor strength of the flanking ligands decreases, while all three complexes maintain excellent consistency between the experimental and theoretical IVCT bands on the high-energy side. Since the IVCT band of $[\mathbf{1}_{\mathbf{Me}}\text{-}\mathbf{Co}]^{3+}$ is only mildly truncated, we assign this complex to a Class IIB description. It is more difficult to distinguish between Class IIB and borderline Class II/III descriptions for $[\mathbf{1}_{\mathbf{H}}\text{-}\mathbf{Co}]^{3+}$ and $[\mathbf{1}_{\mathbf{Cl}}\text{-}\mathbf{Co}]^{3+}$.[37] Our previous assignment of $[\mathbf{1}_{\mathbf{H}}\text{-}\mathbf{Co}]^{3+}$ as borderline Class II/III was made using methods employed by others[13c,15a,16a,b] to analyze metal-bridged mixed-valence systems, and adding to this evidence, its IVCT band was found to be invariant to changing the solvent from MeCN to water or acetone (Figure S100). The absence of solvatochromism is a strong indicator of a highly delocalized electronic structure,[38] and thus, we maintain our borderline Class II/III description for this complex and, by extension, for $[\mathbf{1}_{\mathbf{Cl}}\text{-}\mathbf{Co}]^{3+}$.

Interestingly, the experimental IVCT band of $[\mathbf{1}_{\mathbf{CO2Me}}\text{-}\mathbf{Co}]^{3+}$ poorly matches the theoretical Gaussian band on both the low-energy and high-energy sides. Truncation of the IVCT band is not supposed to alter the band shape on the high energy side,[3] necessitating a different explanation. Since the experimental ν_{max} of the IVCT band is taken as ν_{max} of the theoretical Gaussian band, and the width of the Gaussian band is derived from ν_{max},[3a] the discrepancy between the experimental and theoretical absorptions suggests that the experimental ν_{max} value is not a good representation of ν_{max} of the corresponding Gaussian curve. In other words, these results suggest that the low-energy portion of the experimental IVCT band is truncated to beyond ν_{max} of the theoretical Class II band, just as expected for a Class III mixed-valence system.[3a,b] Comparison of $\Delta\nu_{1/2}$ of the experimental IVCT band with that of the theoretical Gaussian band offers another method of evaluating the extent of delocalization. The experimental full-width at half maximum ($\Delta\nu_{1/2}$ = 2185 cm^{-1}) is 0.57 times that of the theoretical Gaussian band ($\Delta\nu_{1/2}$ = 3792 cm^{-1}). This ratio is slightly larger than the ≤0.5 limit expected for Class III coupling, but it has been noted that physically realistic IVCT bands are not truncated as sharply as theoretically predicted;[11d] therefore, a value slightly larger than 0.5 is not unreasonable for a Class III system.[10b]

As expected from CV data, full or partial 2 e^- reduction of $[\mathbf{2}\text{-}\mathbf{Co}]^{5+}$ does not produce spectra showing signs of electronic coupling (Figure 4). Instead, the 3+ spectrum exhibits features that closely resemble those of fully organic viologen radical cations,[21] even more so than we reported for the zinc complex $[\mathbf{1}_{\mathbf{H}}\text{-}\mathbf{Zn}]^{2+}$.[6a] Since $[\mathbf{2}\text{-}\mathbf{Co}]^{3+}$ is not mixed valence, it is the absence of an IVCT band in the partially reduced sample (Figure 4, −1.08 V, initial) that confirms that the viologen units of $[\mathbf{2}\text{-}\mathbf{Co}]^{n+}$ are electronically isolated. Notably, this observation extends the electronic coupling in the cobaltoviologens all the way from completely localized Class I to fully delocalized Class III, with considerable gradation between these extremes, thus demonstrating an unprecedented degree of control over delocalization in a constant L-M-L core.

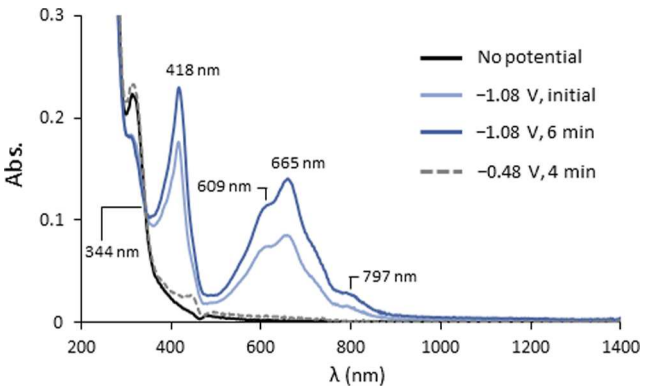

Figure 4. Spectroelectrochemistry of the reduction of $[\mathbf{2}\text{-}\mathbf{Co}]^{5+}$ to $[\mathbf{2}\text{-}\mathbf{Co}]^{3+}$ (0.5 mM in MeCN) at −1.08 V vs $Fc^{+/0}$ in a 1 mm pathlength cuvette, followed by reoxidation at −0.48 V. An isosbestic point is observed at 344 nm.

The spectra of the 2+ and 1+ states of the $[\mathbf{1}_{\mathbf{X}}\text{-}\mathbf{Co}]^{n+}$ series were also acquired. The 2+ states all have similar vis-NIR features to those reported[6a] for $[\mathbf{1}_{\mathbf{H}}\text{-}\mathbf{Co}]^{2+}$ (Figures S79, S83, S87, S91, and S96), though the NMe_2 and CO_2Me derivatives differ somewhat more than the examples from $[\mathbf{1}_{\mathbf{Cl}}\text{-}\mathbf{Co}]^{2+}$ to $[\mathbf{1}_{\mathbf{OMe}}\text{-}\mathbf{Co}]^{2+}$. The 1+ spectra are also fairly consistent for each complex (Figures S80, S84, S88, S92, and S97), in this case with the Cl and CO_2Me derivatives being modest outliers with somewhat broader, more intense bands. Neither the $[\mathbf{1}_{\mathbf{X}}\text{-}\mathbf{Co}]^{2+}$ nor the $[\mathbf{1}_{\mathbf{X}}\text{-}\mathbf{Co}]^{1+}$ spectra suggest dramatic changes in electronic structure across each series, and changes observed for the 1+ spectra are not consistent with changes in inter-ligand electronic coupling, consistent with the narrow range of $\Delta E_{red3,4}$ values for the $[\mathbf{1}_{\mathbf{X}}\text{-}\mathbf{Co}]^{n+}$ complexes.

Single-Crystal X-ray Diffraction and Radical Stacking. As we have reported, structural data support the description of $[\mathbf{1}_{\mathbf{H}}\text{-}\mathbf{Co}]^{3+}$ as a nearly fully delocalized mixed-valence system.[6a] Thus, single-crystal XRD characterization of $[\mathbf{1}_{\mathbf{H}}\text{-}\mathbf{Co}]^{2+}$ and $[\mathbf{1}_{\mathbf{H}}\text{-}\mathbf{Co}]^{+}$ was carried out to similarly bolster our understanding of these states, especially since common DFT methods were found to exhibit significant limitations for characterizing the cobaltoviologens (see Computational Results in the Supporting Information).[35] Two crystals of $[\mathbf{1}_{\mathbf{H}}\text{-}\mathbf{Co}](PF_6)_2$ were analyzed, one grown from PhCN (R_1 = 4.53%, Figure 5) and the other from MeCN (R = 8.47%, Figure 6). Diffraction data was somewhat poor for the latter structure due to the thin, air-sensitive crystals available, but we present this structure because it includes two unique equivalents of $[\mathbf{1}_{\mathbf{H}}\text{-}\mathbf{Co}]^{2+}$ that engage in notable intermolecular

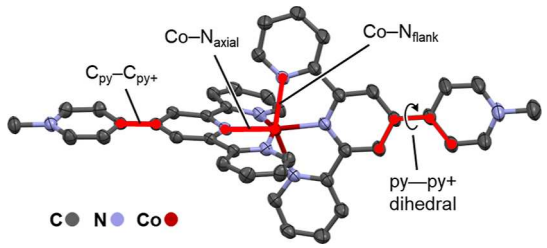

Figure 5. Structure of $[\mathbf{1}_{\mathbf{H}}\text{-}\mathbf{Co}]^{2+}$ determined by XRD (R_1 = 4.53%) on a single crystal of $[\mathbf{1}_{\mathbf{H}}\text{-}\mathbf{Co}](PF_6)_2$ grown by vapor diffusion of Et_2O into a PhCN solution of the salt. Anions and solvates are omitted for clarity. Labels identify the bonds and torsion angles compared in Table 2 for the n = 1−3 states of $[\mathbf{1}_{\mathbf{H}}\text{-}\mathbf{Co}]^{n+}$.

https://doi.org/10.1021/jacs.3c03725
J. Am. Chem. Soc. 2023, 145, 15924−15935

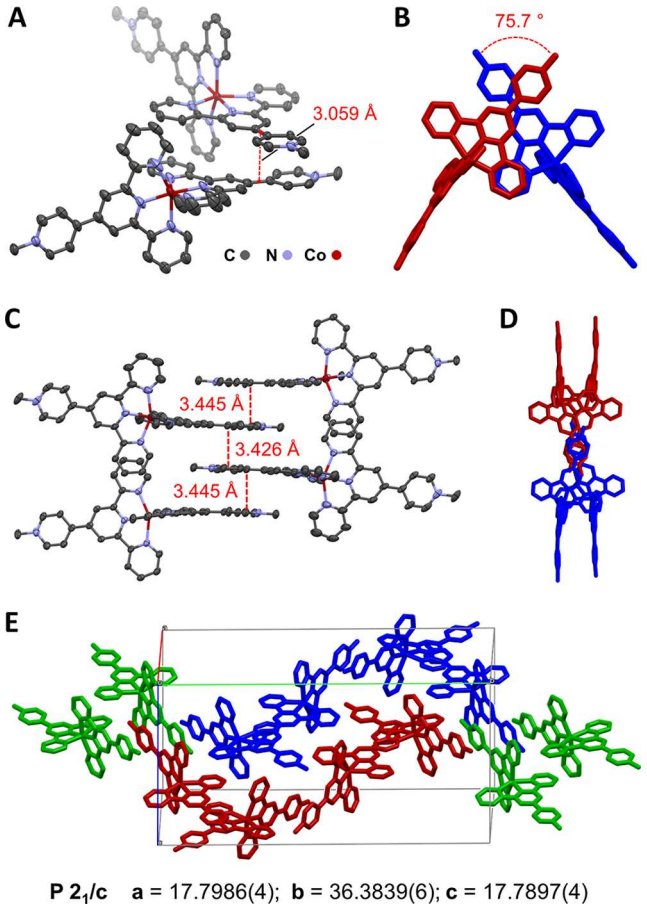

Figure 6. Structure of $[\mathbf{1_H}\text{-}\mathbf{Co}](PF_6)_2{\cdot}3.5MeCN$ determined by single-crystal XRD (R_1 = 8.47%). Anions and solvates are omitted for clarity. (A) Asymmetric unit showing close contact between two crystallographically unique equivalents of $[\mathbf{1_H}\text{-}\mathbf{Co}]^{2+}$. (B) Top-down view of the stacked viologen ligands in the asymmetric unit. (C) Stacking of four viologen ligands in the extended packing structure. (D) View down the stack of four viologen ligands. Red and blue colors are used to distinguish alternating equivalents of $[\mathbf{1_H}\text{-}\mathbf{Co}]^{2+}$. (E) Extended chains of π-stacking between $[\mathbf{1_H}\text{-}\mathbf{Co}]^{2+}$ complexes in the unit cell. Red and blue colors are used to distinguish two separate chains of complexes in the unit cell, and green represents complexes outside the unit cell that unite the two chains in the cell.

interactions (vide infra). A single high-quality structure of $[\mathbf{1_H}\text{-}\mathbf{Co}]PF_6$ was also determined (R_1 = 4.39%, see Figure S108).

The central C−C bond distances and dihedral angles of viologens decrease upon reduction,[21b,33a] so these metrics were compared for the $[\mathbf{1_H}\text{-}\mathbf{Co}]^{n+}$ series. As expected, the pyridine−pyridinium (C_{py}−C_{py+}) bond distances and the py−py+ dihedral angles decrease for both ligands upon increasing reduction of the complex (Table 2), though the change in the C_{py}−C_{py+} distances is only distinguishable beyond experimental error for the 1+ state. These results confirm increasing reduction of the viologen cores of both ligands for each electron added to $[\mathbf{1_H}\text{-}\mathbf{Co}]^{n+}$, with the relative subtlety of the changes presumably reflecting the distribution of each electron across both ligands. Reduction also influences the coordination sphere around cobalt, with all Co−N distances increasing from the 3+ to 2+ states of the complex, though remaining essentially constant between the 2+ and 1+ states. The increased Co−N distances suggest increased metal reduction in the 2+ and 1+ states, though the Co−N distances are not

Table 2. Analysis of the Structural Parameters of $[\mathbf{1_X}\text{-}\mathbf{Co}]^{n+}$

complex	C_{py}−C_{py+} distance (Å)	py−py+ dihedral (°)	Co−N_{axial} distance (Å)	Co−N_{flank} distance (Å)
$[\mathbf{1_H}\text{-}\mathbf{Co}]^{3+}$	1.442(6)[a]	11.1(7)[a]	1.941(3)[a]	2.052(4)[a]
				2.062(4)[a]
$[\mathbf{1_H}\text{-}\mathbf{Co}]^{2+}$	1.429(5)−1.439(4)[b]	3.4(6)[c]	1.978(6)−2.058(6)[b]	2.131(3)−1.171(4)[d]
		3.0(4)[c]		
$[\mathbf{1_H}\text{-}\mathbf{Co}]^{1+}$	1.412(2)	0.6(2)	2.0105(9)	2.142(1)
	1.424(2)	0.8(2)	1.9630(9)	2.150(1)
				2.147(1)
				2.159(1)

[a]Related to a symmetry-equivalent bond/angle by a twofold rotation. [b]Shortest to longest of six distances from three unique $[\mathbf{1_H}\text{-}\mathbf{Co}]^{2+}$ units. [c]Values from the structure of $[\mathbf{1_H}\text{-}\mathbf{Co}](PF_6)_2$ without radical pairing interactions. [d]Shortest to longest of 12 distances from 3 unique $[\mathbf{1_H}\text{-}\mathbf{Co}]^{2+}$ units.

particularly long compared to those of bis-terpy-Co(II) complexes,[26a] consistent with the previous assignment of each reduction as mostly ligand-centered. Notably, C−C and C−N bond distances involving the flanking pyridyl groups (Table S6) do not change meaningfully across all oxidation states of $[\mathbf{1_H}\text{-}\mathbf{Co}]^{n+}$, whereas these bonds are altered substantially upon reduction of typical terpy ligands.[39] This observation confirms that the redox activity of $\mathbf{1_H}^+$ is confined to the viologen-like core rather than involving the *NNN* chelate around the metal.

Interestingly, in crystals of $[\mathbf{1_H}\text{-}\mathbf{Co}]^{2+}$ grown from MeCN ($[\mathbf{1_H}\text{-}\mathbf{Co}](PF_6)_2{\cdot}3.5MeCN$), the complexes engage in π-stacking interactions between the viologen ligands that are characteristic of radical pimerization of organic viologens.[21] The asymmetric unit (Figure 6A,B) includes two unique $[\mathbf{1_H}\text{-}\mathbf{Co}]^{2+}$ complexes, each with a viologen ligand crossing the other at their C_{py}−C_{py+} bonds to give a short centroid-to-centroid contact of 3.06 Å and a dihedral angle of 75.7° between the ligands at this contact. This geometry is nearly ideal for the orbital mixing that produces a weak covalent bonding interaction between organic viologen radicals.[21a,40] Such interactions can facilitate through-space delocalization[41] of electrons across multiple viologens,[23b] yielding unique electronic properties in discrete stacks of viologens[23c,d] and semiconductor behavior in continuous crystalline lattices.[23a] Despite the importance of these interactions in traditional viologen radicals, such behavior has never previously been characterized in metalloviologens, representing a notable fundamental discovery.[42]

The extended packing of the complexes reveals a second notable π-stacking motif (Figure 6C,D) in which four ligands are arranged together with a separation between them (>3.4 Å) that is characteristic of van der Waals contacts in the absence of radical pairing. Consistent with this description, overlap of the ligands is limited mostly to the pyridinium groups and occurs at a very wide angle (Figure 6D), yielding poor alignment for mixing the singly occupied orbitals of each ligand. Interestingly, these quadruple stacks of ligands serve as nodes that crosslink separate chains of cobaltoviologen complexes in the extended packing of $[\mathbf{1_H}\text{-}\mathbf{Co}](PF_6)_2{\cdot}3.5MeCN$ (Figure 6E). The resulting 3-dimensional network of π-stacking interactions appears to impart remarkable elastic flexibility to the bulk crystals,[43] producing needle-like crystals that can recover from being bent by as much as 90° (see Supporting Videos). However, crystals of $[\mathbf{1_H}\text{-}\mathbf{Co}](PF_6)_2{\cdot}$

https://doi.org/10.1021/jacs.3c03725
J. Am. Chem. Soc. 2023, 145, 15924−15935

3.5MeCN quickly become fragile once removed from their supernatant, so far limiting further scrutiny of their elastic properties.

It is worth noting that one viologen ligand of each $[\mathbf{1_H\text{-}Co}]^{2+}$ complex engages in strong radical-dimerization, while the opposite ligand enters into the quadruple-stack motif with weaker π-stacking. The alternating behavior of the ligands might arise from the electronic structure of $[\mathbf{1_H\text{-}Co}]^{2+}$, which features one ligand radical coupled ferromagnetically to cobalt while the other couples antiferromagnetically.[6a] Since this latter interaction pairs the π^* radical with the metal, it may render the ligand unable to participate in intermolecular radical−radical interactions while leaving available the strong van der Waals forces that also play an important role in viologen pimerization.[21a] Thus, metal−ligand electronic interactions in $[\mathbf{1_H\text{-}Co}]^{2+}$ may contribute to the packing motif seen in these crystals, and by extension, their unusual physical properties.

The zinc complex $[\mathbf{1_H\text{-}Zn}]^{2+}$, which has two radical ligands and a closed-shell metal, serves as an obvious experimental control for understanding how metal−ligand electronic coupling influences intermolecular radical pairing. Like the cobalt analogue, $[\mathbf{1_H\text{-}Zn}](PF_6)_2$ can be crystallized from MeCN to yield a packing structure defined by radical pimerization (Figure 7), while these interactions are absent

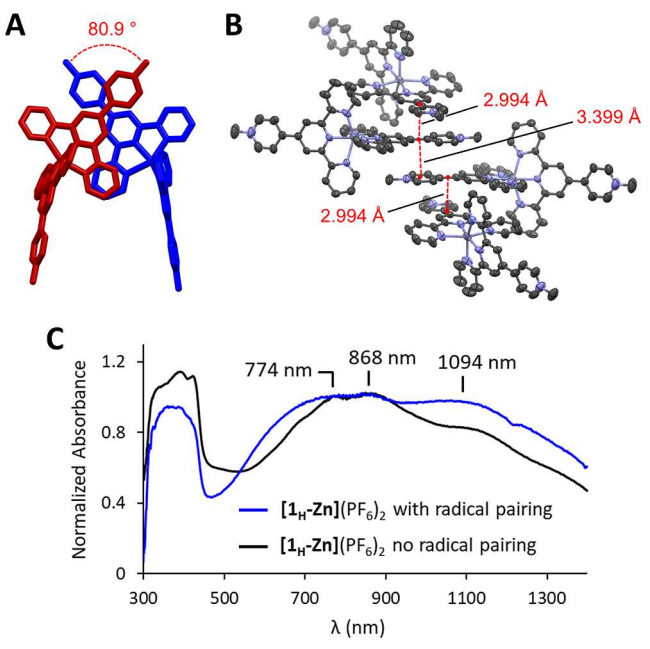

Figure 7. (A) Structure of $[\mathbf{1_H\text{-}Zn}]^{2+}$ determined by XRD (R_1 = 7.97%) on a single crystal of $[\mathbf{1_H\text{-}Zn}](PF_6)_2\cdot$3MeCN. The asymmetric unit is shown with anions and solvates omitted. (B) Quadruple-stack of viologen units observed in the extended packing of $[\mathbf{1_H\text{-}Zn}](PF_6)_2\cdot$3MeCN. (C) Diffuse-reflectance UV−vis−NIR spectra of solid-state samples of $[\mathbf{1_H\text{-}Zn}](PF_6)_2$ with and without radical pairing interactions.

in crystals grown from PhCN (Figure S109). However, packing in the MeCN structures differs considerably between the cobalt and zinc derivatives, with the latter engaging both ligands of each complex in radical-pairing interactions, as expected since both ligand radicals should be equivalent in $[\mathbf{1_H\text{-}Zn}]^{2+}$. The distance of ∼2.99 Å and angle of 80.9° between the stacked ligands are consistent with strong radical pairing, but the extended structure still reveals stacks of four viologens—one viologen unit in each radical dimer also engages in van der Waals contacts (3.399 Å) with one of the viologens of a neighboring radical dimer (Figure 7B). Thus, paired radical ligands maintain the ability to engage in further π-stacking, just without the benefit of additional radical−radical interactions.[44] These observations appear to support the conjecture that the reason only one ligand in $[\mathbf{1_H\text{-}Co}]^{2+}$ engages in strong radical pimerization is that the other ligand π^* electron pairs antiferromagnetically with the cobalt center.

The π-stacking in $[\mathbf{1_H\text{-}Zn}](PF_6)_2$ provides a three-dimensionally extended network of stacking interactions, again leading to elastically flexible crystals (see the Supporting Video). Since the π-stacking networks differ considerably between the zinc and cobalt crystals, it seems that the combination of terpyridine coordination chemistry, radical-pairing interactions, and traditional π-stacking may be more important than the specific topology of these interactions for supporting mechanical flexibility. As with the cobalt analogue, the crystals of $[\mathbf{1_H\text{-}Zn}](PF_6)_2$ lose their integrity quickly outside of solvent, preventing further study of their mechanical properties. However, it was possible to use diffuse reflectance UV−vis−NIR spectroscopy to demonstrate that radical pairing interactions are maintained even after degradation of the crystals. An increased NIR absorbance and broadened visible region band, which are both characteristic of viologen radical dimerization,[21a] were observed for dried samples of crystals featuring the radical-pairing motif in comparison to crystals grown under conditions that do not lead to radical pairing (Figure 7C).

SUMMARY AND CONCLUSIONS

We have prepared a series of metalloviologen complexes $[\mathbf{1_X\text{-}M}]^{n+}$ and $[\mathbf{2\text{-}Co}]^{5+}$ in which two viologen-like redox units are bridged by either a cobalt or zinc ion. Notably, the mixed-valence states of the cobaltoviologens could be tuned all the way from fully localized Class I to fully delocalized Class III descriptions, providing the first L-M-L system in which this full range of states could be achieved while maintaining a fixed set of redox-active units and bridging metal. This remarkable control over electronic coupling results from a novel tuning strategy in which ancillary ligands are used to modulate the electronics of the cobalt center while leaving the viologen units relatively unperturbed. This approach allows the energies of high-spin Co^{II} orbitals to be matched to those of the viologens to maximize delocalization, while at the other extreme, electronic coupling is turned off when the cobalt ion is perturbed enough to change its oxidation state to low-spin Co^{III}. In another notable finding, the viologen-like ligands can engage in intermolecular radical-pairing interactions in crystals of $[\mathbf{1_H\text{-}Co}]^{2+}$ and $[\mathbf{1_H\text{-}Zn}]^{2+}$. This discovery represents the first time that metalloviologen complexes have been observed to engage in the type of radical π-stacking that has proven valuable to the development of electronic materials and molecular machines using organic viologens.

The combination of simple pyridine-based coordination chemistry, highly tunable intramolecular electronic delocalization, and π-radical-pairing interactions provide the cobaltoviologens with a unique set of features that are likely to be valuable for the development of materials with novel electronic and/or mechanical properties. First, by overcoming limitations to tunability seen in other MV systems, the cobaltoviologens may be useful for developing new electronic materials, especially

https://doi.org/10.1021/jacs.3c03725
J. Am. Chem. Soc. 2023, 145, 15924−15935

since these complexes are isostructural with other (4′-Ar-terpy)$_2$M^{2+} complexes that are already well-established components of a variety of notable (nano)materials.[45] Likewise, the combination of terpyridine coordination chemistry and π-radical pairing is promising for the development of materials with emergent properties. Indeed, radical π-stacking leads $[\mathbf{1_H}\text{-}\mathbf{Co}]^{2+}$ and $[\mathbf{1_H}\text{-}\mathbf{Zn}]^{2+}$ to assemble into 3D crystalline networks that exhibit elastic flexibility not seen in organic viologen radical crystals, providing an initial confirmation that the metalloviologens may be useful for creating materials with properties beyond those of their individual components.

■ ASSOCIATED CONTENT

Supporting Information

The Supporting Information is available free of charge at https://pubs.acs.org/doi/10.1021/jacs.3c03725.

Flexible crystals of $[\mathbf{1_H}\text{-}\mathbf{Co}](PF_6)_2\cdot 3.5MeCN$ (MP4)
Ninety degree bend of crystal of $[\mathbf{1_H}\text{-}\mathbf{Co}](PF_6)_2\cdot 3.5MeCN$ (MP4)
Flexible crystals of $[\mathbf{1_H}\text{-}\mathbf{Zn}](PF_6)_2\cdot 3MeCN$ (MP4)
Synthetic and experimental procedures; NMR (^{1}H, ^{13}C{^{1}H}), UV−vis−NIR, and ESI(+)-MS spectra; cyclic voltammograms; single-crystal X-ray diffraction data and analysis; and details of DFT calculations (PDF)

Accession Codes

CCDC 2255265−2255269 contain the supplementary crystallographic data for this paper. These data can be obtained free of charge via www.ccdc.cam.ac.uk/data_request/cif, or by emailing data_request@ccdc.cam.ac.uk, or by contacting The Cambridge Crystallographic Data Centre, 12 Union Road, Cambridge CB2 1EZ, UK; fax: +44 1223 336033.

■ AUTHOR INFORMATION

Corresponding Author

Mark C. Lipke − *Department of Chemistry and Chemical Biology, Rutgers, The State University of New Jersey, Piscataway, New Jersey 08854, United States;* orcid.org/0000-0003-0035-4565; Email: ml1353@chem.rutgers.edu

Authors

Brice J. O. Kessler − *Department of Chemistry and Chemical Biology, Rutgers, The State University of New Jersey, Piscataway, New Jersey 08854, United States;* orcid.org/0000-0003-2633-8272

Iram F. Mansoor − *Department of Chemistry and Chemical Biology, Rutgers, The State University of New Jersey, Piscataway, New Jersey 08854, United States*

Derek I. Wozniak − *Department of Chemistry and Chemical Biology, Rutgers, The State University of New Jersey, Piscataway, New Jersey 08854, United States*

Thomas J. Emge − *Department of Chemistry and Chemical Biology, Rutgers, The State University of New Jersey, Piscataway, New Jersey 08854, United States*

Complete contact information is available at: https://pubs.acs.org/10.1021/jacs.3c03725

Author Contributions

All authors have given approval to the final version of the manuscript.

Notes

The authors declare no competing financial interest.

■ ACKNOWLEDGMENTS

The authors acknowledge Rutgers, The State University of New Jersey, for financial support of this research; the Office of Advanced Research Computing (OARC) at Rutgers, The State University of New Jersey, for providing access to the Amarel cluster and associated research computing resources; and the National Science Foundation MRI Program Award 2117792 for supporting the purchase of a single-crystal X-ray diffractometer employed in this research. I.F.M. acknowledges the National Science Foundation Graduate Research Fellowship Program for support via Award DGE-2233066.

■ REFERENCES

(1) For recent reviews: (a) Heckmann, A.; Lambert, C. Organic Mixed-Valence Compounds: A Playground for Electrons and Holes. *Angew. Chem., Int. Ed.* **2012**, *51*, 326−392. (b) Hankache, J.; Wenger, O. S. Organic Mixed Valence. *Chem. Rev.* **2011**, *111*, 5138−5178. (c) Launay, J.-P. Mixed-Valent Compounds and Their Properties − Recent Developments. *Eur. J. Inorg. Chem.* **2020**, *2020*, 329−341.

(2) (a) Gross, S. T. The Crystal Structure of Pb_3O_4. *J. Am. Chem. Soc.* **1943**, *65*, 1107−1110. (b) Mazej, Z.; Michałowski, T.; Goreshnik, E. A.; Jagličić, Z.; Arčon, I.; Szydłowska, J.; Grochala, W. The first example of a mixed valence ternary compound of silver with random distribution of Ag(i) and Ag(ii) cations. *Dalton Trans.* **2015**, *44*, 10957−10968. (c) Intrator, J. A.; Orchanian, N. M.; Clough, A. J.; Haiges, R.; Marinescu, S. C. Electronically-coupled redox centers in trimetallic cobalt complexes. *Dalton Trans.* **2022**, *51*, 5660−5672. (d) Coropceanu, V.; Gruhn, N. E.; Barlow, S.; Lambert, C.; Durivage, J. C.; Bill, T. G.; Nöll, G.; Marder, S. R.; Brédas, J.-L. Electronic Couplings in Organic Mixed-Valence Compounds: The Contribution of Photoelectron Spectroscopy. *J. Am. Chem. Soc.* **2004**, *126*, 2727−2731. (e) Creutz, C.; Taube, H. Direct Approach to Measuring the Franck-Condon Barrier to Electron Transfer between Metal Ions. *J. Am. Chem. Soc.* **1969**, *91*, 3988−3989. (f) Hernández Sánchez, R.; Zheng, S.-L.; Betley, T. A. Ligand Field Strength Mediates Electron Delocalization in Octahedral $[(^{H}L)_2Fe_6(L')_m]^{n+}$ Clusters. *J. Am. Chem. Soc.* **2015**, *137*, 11126−11143. (g) Storr, T.; Wasinger, E. C.; Pratt, R. C.; Stack, T. D. P. The Geometric and Electronic Structure of a One-Electron-Oxidized Nickel(II) Bis-(Salicylidene)Diamine Complex. *Angew. Chem., Int. Ed.* **2007**, *46*, 5198−5201.

(3) (a) Brunschwig, B. S.; Creutz, C.; Sutin, N. Optical transitions of symmetrical mixed-valence systems in the Class II−III transition regime. *Chem. Soc. Rev.* **2002**, *31*, 168−184. (b) D'Alessandro, D. M.; Keene, F. R. Current Trends and Future Challenges in the Experimental, Theoretical and Computational Analysis of Intervalence Charge Transfer (IVCT) Transitions. *Chem. Soc. Rev.* **2006**, *35*, 424−440. (c) Demadis, K. D.; Hartshorn, C. M.; Meyer, T. J. The Localized-to-Delocalized Transition in Mixed-Valence Chemistry. *Chem. Rev.* **2001**, *101*, 2655−2686. (d) Launay, J.-P. Long-distance intervalence electron transfer. *Chem. Soc. Rev.* **2001**, *30*, 386−397.

(4) (a) Sampaio, R. N.; Piechota, E. J.; Troian-Gautier, L.; Maurer, A. B.; Hu, K.; Schauer, P. A.; Blair, A. D.; Berlinguette, C. P.; Meyer, G. J. Kinetics Teach That Electronic Coupling Lowers the Free-Energy Change That Accompanies Electron Transfer. *Proc. Natl. Acad. Sci. U.S.A.* **2018**, *115*, 7248−7253. (b) Luo, Y.; Tran, J. H.; Wächtler, M.; Schulz, M.; Barthelmes, K.; Winter, A.; Rau, S.; Schubert, U. S.; Dietzek, B. Remote Control of Electronic Coupling − Modification of Excited-State Electron-Transfer Rates in $Ru(Tpy)_2$-Based Donor−Acceptor Systems by Remote Ligand Design. *Chem. Commun.* **2019**, *55*, 2273−2276. (c) Al-Faouri, T.; Buguis, F. L.; Azizi Soldouz, S.; Sarycheva, O. V.; Hussein, B. A.; Mahmood, R.; Koivisto, B. D. Exploring Structure-Property Relationships in a Bio-Inspired Family of Bipodal and Electronically-Coupled Bistriphenylamine Dyes for Dye-Sensitized Solar Cell Applications. *Molecules* **2020**, *25*, 2260.

(5) (a) Xie, L. S.; Sun, L.; Wan, R.; Park, S. S.; DeGayner, J. A.; Hendon, C. H.; Dincă, M. Tunable Mixed-Valence Doping toward

Record Electrical Conductivity in a Three-Dimensional Metal−Organic Framework. *J. Am. Chem. Soc.* **2018**, *140*, 7411−7414. (b) Murase, R.; Hudson, T. A.; Aldershof, T. S.; Nguyen, K. V.; Gluschke, J. G.; Kenny, E. P.; Zhou, X.; Wang, T.; van Koeverden, M. P.; Powell, B. J.; Micolich, A. P.; Abrahams, B. F.; D'Alessandro, D. M. Multi-Redox Responsive Behavior in a Mixed-Valence Semiconducting Framework Based on Bis-[1,2,5]-Thiadiazolo-Tetracyanoquinodimethane. *J. Am. Chem. Soc.* **2022**, *144*, 13242−13253. (c) Ziebel, M. E.; Darago, L. E.; Long, J. R. Control of Electronic Structure and Conductivity in Two-Dimensional Metal−Semiquinoid Frameworks of Titanium, Vanadium, and Chromium. *J. Am. Chem. Soc.* **2018**, *140*, 3040−3051. (d) Clough, A. J.; Orchanian, N. M.; Skelton, J. M.; Neer, A. J.; Howard, S. A.; Downes, C. A.; Piper, L. F. J.; Walsh, A.; Melot, B. C.; Marinescu, S. C. Room Temperature Metallic Conductivity in a Metal−Organic Framework Induced by Oxidation. *J. Am. Chem. Soc.* **2019**, *141*, 16323−16330. (e) Clough, A. J.; Skelton, J. M.; Downes, C. A.; de la Rosa, A. A.; Yoo, J. W.; Walsh, A.; Melot, B. C.; Marinescu, S. C. Metallic Conductivity in a Two-Dimensional Cobalt Dithiolene Metal−Organic Framework. *J. Am. Chem. Soc.* **2017**, *139*, 10863−10867.

(6) (a) Mansoor, I. F.; Wozniak, D. I.; Wu, Y.; Lipke, M. C. A Delocalized Cobaltoviologen with Seven Reversibly Accessible Redox States and Highly Tunable Electrochromic Behaviour. *Chem. Commun.* **2020**, *56*, 13864−13867. (b) Cui, B.-B.; Tang, J.-H.; Yao, J.; Zhong, Y.-W. A Molecular Platform for Multistate Near-Infrared Electrochromism and Flip-Flop, Flip-Flap-Flop, and Ternary Memory. *Angew. Chem., Int. Ed.* **2015**, *54*, 9192−9197. (c) Rogez, G.; Marvilliers, A.; Sarr, P.; Parsons, S.; Teat, S. J.; Ricard, L.; Mallah, T. Tuning the Optical Properties of Prussian Blue-like Complexes. *Chem. Commun.* **2002**, 1460−1461. (d) Weyland, T.; Ledoux, I.; Brasselet, S.; Zyss, J.; Lapinte, C. Nonlinear Optical Properties of Redox-Active Mono-Bi-and Trimetallic σ-Acetylide Complexes Connected through a Phenyl Ring in the Cp*(Dppe)Fe Series. An Example of Electro-Switchable NLO Response. *Organometallics* **2000**, *19*, 5235−5237.

(7) (a) Kaim, W.; Klein, A.; Glöckle, M. Exploration of Mixed-Valence Chemistry: Inventing New Analogues of the Creutz-Taube Ion. *Acc. Chem. Res.* **2000**, *33*, 755−763. (b) Silva, W. C.; Lima, J. B.; Moreira, I. S.; Neto, A. M.; Gandra, F. C. G.; Ferreira, A. G.; McGarvey, B. R.; Franco, D. W. 4,4'-Dithiodipyridine as a Bridging Ligand in Osmium and Ruthenium Complexes: The Electron Conductor Ability of the −S−S− Bridge. *Inorg. Chem.* **2003**, *42*, 6898−6906.

(8) (a) Gao, H.; Mallick, S.; Cao, L.; Meng, M.; Cheng, T.; Chen, H. W.; Liu, C. Y. Electronic Coupling and Electron Transfer between Two Mo_2 Units through Meta- and Para-Phenylene Bridges. *Chem.—Eur. J.* **2019**, *25*, 3930−3938. (b) Patoux, C.; Launay, J.-P.; Beley, M.; Chodorowski-Kimmes, S.; Collin, J.-P.; James, S.; Sauvage, J.-P. Long-Range Electronic Coupling in Bis(Cyclometalated) Ruthenium Complexes. *J. Am. Chem. Soc.* **1998**, *120*, 3717−3725. (c) Sutton, J. E.; Taube, H. Metal to Metal Interactions in Weakly Coupled Mixed-Valence Complexes Based on Ruthenium Ammines. *Inorg. Chem.* **1981**, *20*, 3125−3134. (d) Cao, Z.; Xi, B.; Jodoin, D. S.; Zhang, L.; Cummings, S. P.; Gao, Y.; Tyler, S. F.; Fanwick, P. E.; Crutchley, R. J.; Ren, T. Diruthenium-Polyyn-diyl-Diruthenium Wires: Electronic Coupling in the Long Distance Regime. *J. Am. Chem. Soc.* **2014**, *136*, 12174−12183.

(9) (a) Shao, J.-Y.; Zhong, Y.-W. Tuning the Electronic Coupling in Cyclometalated Diruthenium Complexes through Substituent Effects: A Correlation between the Experimental and Calculated Results. *Chem.—Eur. J.* **2014**, *20*, 8702−8713. (b) Kundu, T.; Schweinfurth, D.; Sarkar, B.; Mondal, T. K.; Fiedler, J.; Mobin, S. M.; Puranik, V. G.; Kaim, W.; Lahiri, G. K. Strong Metal−Metal Coupling in Mixed-Valent Intermediates $[Cl(L)Ru(\mu\text{-}Tppz)Ru(L)Cl]^+$, L = β-Diketonato Ligands, Tppz = 2,3,5,6-Tetrakis(2-Pyridyl)Pyrazine. *Dalton Trans.* **2012**, *41*, 13429−13440. (c) Scheiring, T.; Kaim, W.; Olabe, J. A.; Parise, A. R.; Fiedler, J. The Valence-Localized Decacyanodiruthenium(III,II) Analogue of the Creutz−Taube Ion. Completing the Full D^5/D^6 Triad $[(NC)_5M(\mu\text{-}Pz)M(CN)_5]^{5-}$, M=Fe,Ru,Os; Pz=pyrazine. *Inorganica Chim. Acta* **2000**, *300*−*302*, 125−130. (d) Vance, F. W.; Slone, R. V.; Stern, C. L.; Hupp, J. T. Comparative Absorption, Electroabsorption and Electrochemical Studies of Intervalence Electron Transfer and Electronic Coupling in Cyanide-Bridged Bimetallic Systems: Ancillary Ligand Effects. *Chem. Phys.* **2000**, *253*, 313−322.

(10) (a) Hansmann, M. M.; Melaimi, M.; Bertrand, G. Organic Mixed Valence Compounds Derived from Cyclic (Alkyl)(Amino)-Carbenes. *J. Am. Chem. Soc.* **2018**, *140*, 2206−2213. (b) Barlow, S.; Risko, C.; Odom, S. A.; Zheng, S.; Coropceanu, V.; Beverina, L.; Brédas, J.-L.; Marder, S. R. Tuning Delocalization in the Radical Cations of 1,4-Bis[4-(Diarylamino)Styryl]Benzenes, 2,5-Bis[4-(Diarylamino)Styryl]Thiophenes, and 2,5-Bis[4-(Diarylamino)-Styryl]Pyrroles through Substituent Effects. *J. Am. Chem. Soc.* **2012**, *134*, 10146−10155. (c) Yu, C.-H.; Zhu, C.; Ji, X.; Hu, W.; Xie, H.; Bhuvanesh, N.; Fang, L.; Ozerov, O. V. Palladium Bis-Pincer Complexes with Controlled Rigidity and Inter-Metal Distance. *Inorg. Chem. Front.* **2020**, *7*, 4357−4366.

(11) (a) Schäfer, J.; Holzapfel, M.; Mladenova, B.; Kattnig, D.; Krummenacher, I.; Braunschweig, H.; Grampp, G.; Lambert, C. Hole Transfer Processes in Meta- and Para-Conjugated Mixed Valence Compounds: Unforeseen Effects of Bridge Substituents and Solvent Dynamics. *J. Am. Chem. Soc.* **2017**, *139*, 6200−6209. (b) Jung, H. W.; Yoon, S. E.; Carroll, P. J.; Gau, M. R.; Therien, M. J.; Kang, Y. K. Distance Dependence of Electronic Coupling in Rigid, Cofacially Compressed, π-Stacked Organic Mixed-Valence Systems. *J. Phys. Chem. B* **2020**, *124*, 1033−1048. (c) Rovira, C.; Ruiz-Molina, D.; Elsner, O.; Vidal-Gancedo, J.; Bonvoisin, J.; Launay, J.-P.; Veciana, J. Influence of Topology on the Long-Range Electron-Transfer Phenomenon. *Chem.—Eur. J.* **2001**, *7*, 240−250. (d) Lambert, C.; Nöll, G. The Class II/III Transition in Triarylamine Redox Systems. *J. Am. Chem. Soc.* **1999**, *121*, 8434−8442. (e) Barlow, S.; Risko, C.; Chung, S.-J.; Tucker, N. M.; Coropceanu, V.; Jones, S. C.; Levi, Z.; Brédas, J.-L.; Marder, S. R. Intervalence Transitions in the Mixed-Valence Monocations of Bis(triarylamines) Linked with Vinylene and Phenylene−Vinylene Bridges. *J. Am. Chem. Soc.* **2005**, *127*, 16900−16911.

(12) Lambert, C.; Amthor, S.; Schelter, J. From Valence Trapped to Valence Delocalized by Bridge State Modification in Bis-(Triarylamine) Radical Cations: Evaluation of Coupling Matrix Elements in a Three-Level System. *J. Phys. Chem. A* **2004**, *108*, 6474−6486.

(13) (a) Jones, S. C.; Coropceanu, V.; Barlow, S.; Kinnibrugh, T.; Timofeeva, T.; Brédas, J.-L.; Marder, S. R. Delocalization in Platinum−Alkynyl Systems: A Metal-Bridged Organic Mixed-Valence Compound. *J. Am. Chem. Soc.* **2004**, *126*, 11782−11783. (b) Kojima, T.; Ogishima, F.; Nishibu, T.; Kotani, H.; Ishizuka, T.; Okajima, T.; Nozawa, S.; Shiota, Y.; Yoshizawa, K.; Ohtsu, H.; Kawano, M.; Shiga, T.; Oshio, H. Intermediate-Spin Iron(III) Complexes Having a Redox-Noninnocent Macrocyclic Tetraamido Ligand. *Inorg. Chem.* **2018**, *57*, 9683−9695. (c) Lu, C. C.; Bill, E.; Weyhermüller, T.; Bothe, E.; Wieghardt, K. Neutral Bis(α-iminopyridine)metal Complexes of the First-Row Transition Ions (Cr, Mn, Fe, Co, Ni, Zn) and Their Monocationic Analogues: Mixed Valency Involving a Redox Noninnocent Ligand System. *J. Am. Chem. Soc.* **2008**, *130*, 3181−3197.

(14) (a) Chiang, L.; Kochem, A.; Jarjayes, O.; Dunn, T. J.; Vezin, H.; Sakaguchi, M.; Ogura, T.; Orio, M.; Shimazaki, Y.; Thomas, F.; Storr, T. Radical Localization in a Series of Symmetric Ni^{II} Complexes with Oxidized Salen Ligands. *Chem.—Eur. J.* **2012**, *18*, 14117−14127. (b) Chiang, L.; Herasymchuk, K.; Thomas, F.; Storr, T. Influence of Electron-Withdrawing Substituents on the Electronic Structure of Oxidized Ni and Cu Salen Complexes. *Inorg. Chem.* **2015**, *54*, 5970−5980. (c) Shimazaki, Y.; Stack, T. D. P.; Storr, T. Detailed Evaluation of the Geometric and Electronic Structures of One-Electron Oxidized Group 10 (Ni, Pd, and Pt) Metal(II)-(Disalicylidene)Diamine Complexes. *Inorg. Chem.* **2009**, *48*, 8383−8392. (d) Kurahashi, T.; Fujii, H. One-Electron Oxidation of Electronically Diverse Manganese(III) and Nickel(II) Salen Complexes: Transition from

https://doi.org/10.1021/jacs.3c03725
J. Am. Chem. Soc. 2023, 145, 15924−15935

Localized to Delocalized Mixed-Valence Ligand Radicals. *J. Am. Chem. Soc.* **2011**, *133*, 8307−8316.
(15) (a) Yu, C.-H.; Yang, X.; Ji, X.; Wang, C.-H.; Lai, Q.; Bhuvanesh, N.; Ozerov, O. V. Redox Communication between Two Diarylamido/Bis(Phosphine) (PNP)M Moieties Bridged by Ynediyl Linkers (M = Ni, Pd, Pt). *Inorg. Chem.* **2020**, *59*, 10153−10162. (b) Hewage, J. S.; Wanniarachchi, S.; Morin, T. J.; Liddle, B. J.; Banaszynski, M.; Lindeman, S. V.; Bennett, B.; Gardinier, J. R. Homoleptic Nickel(II) Complexes of Redox-Tunable Pincer-Type Ligands. *Inorg. Chem.* **2014**, *53*, 10070−10084. (c) Liddle, B. J.; Wanniarachchi, S.; Hewage, J. S.; Lindeman, S. V.; Bennett, B.; Gardinier, J. R. Electronic Communication Across Diamagnetic Metal Bridges: A Homoleptic Gallium(III) Complex of a Redox-Active Diarylamido-Based Ligand and Its Oxidized Derivatives. *Inorg. Chem.* **2012**, *51*, 12720−12728.
(16) (a) Arnold, A.; Sherbow, T. J.; Bohanon, A. M.; Sayler, R. I.; Britt, R. D.; Smith, A. M.; Fettinger, J. C.; Berben, L. A. Delocalization Tunable by Ligand Substitution in $[L_2Al]^{N-}$ Complexes Highlights a Mechanism for Strong Electronic Coupling. *Chem. Sci.* **2021**, *12*, 675−682. (b) Arnold, A.; Sherbow, T. J.; Sayler, R. I.; Britt, R. D.; Thompson, E. J.; Muñoz, M. T.; Fettinger, J. C.; Berben, L. A. Organic Electron Delocalization Modulated by Ligand Charge States in $[L_2M]^{n-}$ Complexes of Group 13 Ions. *J. Am. Chem. Soc.* **2019**, *141*, 15792−15803. (c) de Bruin, B.; Bill, E.; Bothe, E.; Weyhermüller, T.; Wieghardt, K. Molecular and Electronic Structures of Bis(Pyridine-2,6-Diimine)Metal Complexes $[ML_2](PF_6)_n$ (n = 0, 1, 2, 3; M = Mn, Fe, Co, Ni, Cu, Zn). *Inorg. Chem.* **2000**, *39*, 2936−2947.
(17) (a) Ray, K.; Begum, A.; Weyhermüller, T.; Piligkos, S.; van Slageren, J.; Neese, F.; Wieghardt, K. The Electronic Structure of the Isoelectronic, Square-Planar Complexes $[Fe^{II}(L)_2]^{2-}$ and $[Co^{III}(L^{Bu})_2]^-$ (L^{2-} and $(L^{Bu})^{2-}$ = Benzene-1,2-Dithiolates): An Experimental and Density Functional Theoretical Study. *J. Am. Chem. Soc.* **2005**, *127*, 4403−4415. (b) Vogler, A.; Kunkely, H. A 1,2-Dithiolenenickel Complex with Different Substituents-a Novel Type of Mixed-Valence Compounds. *Angew. Chem., Int. Ed. Engl.* **1982**, *21*, 77. (c) Wan, H. C.; Zhang, J.-X.; Leung, C. S.; Sheong, F. K.; Lin, Z. Inter-Ligand Delocalisations in Transition Metal Complexes Containing Multiple Non-Innocent Ligands. *Dalton Trans.* **2019**, *48*, 14801−14807.
(18) It is worth clarifying that cobalt bis-dithiolene complexes are not usually described in terms of mixed valency, but the resonance structures $[Co^{III}(L)_2]^- \leftrightarrow [Co^{II}(L)(L^{\bullet})]^- \leftrightarrow [Co^{II}(L^{\bullet})(L)]^-$ presented in ref 17a can be understood as corresponding to a delocalized MV system with considerable bridge-centered redox character.
(19) (a) Römelt, C.; Weyhermüller, T.; Wieghardt, K. Structural Characteristics of Redox-Active Pyridine-1,6-Diimine Complexes: Electronic Structures and Ligand Oxidation Levels. *Coord. Chem. Rev.* **2019**, *380*, 287−317. (b) Clarke, R. M.; Herasymchuk, K.; Storr, T. Electronic Structure Elucidation in Oxidized Metal−Salen Complexes. *Coord. Chem. Rev.* **2017**, *352*, 67−82. (c) Eisenberg, R.; Gray, H. B. Noninnocence in Metal Complexes: A Dithiolene Dawn. *Inorg. Chem.* **2011**, *50*, 9741−9751.
(20) (a) Chen, K.; Downes, C. A.; Schneider, E.; Goodpaster, J. D.; Marinescu, S. C. Improving and Understanding the Hydrogen Evolving Activity of a Cobalt Dithiolene Metal−Organic Framework. *ACS Appl. Mater. Interfaces* **2021**, *13*, 16384−16395. (b) Downes, C. A.; Marinescu, S. C. Efficient Electrochemical and Photoelectrochemical H_2 Production from Water by a Cobalt Dithiolene One-Dimensional Metal−Organic Surface. *J. Am. Chem. Soc.* **2015**, *137*, 13740−13743.
(21) (a) Geraskina, M. R.; Dutton, A. S.; Juetten, M. J.; Wood, S. A.; Winter, A. H. The Viologen Cation Radical Pimer: A Case of Dispersion-Driven Bonding. *Angew. Chem., Int. Ed.* **2017**, *56*, 9435−9439. (b) Bockman, T. M.; Kochi, J. K. Isolation and Oxidation-Reduction of Methylviologen Cation Radicals. Novel Disproportionation in Charge-Transfer Salts by X-ray Crystallography. *J. Org. Chem.* **1990**, *55*, 4127−4135. (c) Geuder, W.; Hünig, S.; Suchy, A. Single and Double Bridged Viologenes and Intramolecular Pimerization of Their Cation Radicals. *Tetrahedron* **1986**, *42*, 1665−1677.
(22) (a) Ma, W.; Xu, L.; Zhang, S.; Li, G.; Ma, T.; Rao, B.; Zhang, M.; He, G. Phosphorescent Bismoviologens for Electrophosphorochromism and Visible Light-Induced Cross-Dehydrogenative Coupling. *J. Am. Chem. Soc.* **2021**, *143*, 1590−1597. (b) Stolar, M.; Borau-Garcia, J.; Toonen, M.; Baumgartner, T. Synthesis and Tunability of Highly Electron-Accepting, N-Benzylated "Phosphaviologens". *J. Am. Chem. Soc.* **2015**, *137*, 3366−3371. (c) Bridges, C. R.; Borys, A. M.; Béland, V. A.; Gaffen, J. R.; Baumgartner, T. Phosphoryl- and phosphonium-bridged viologens as stable two- and three-electron acceptors for organic electrodes. *Chem. Sci.* **2020**, *11*, 10483−10487.
(23) (a) Fahrenbach, A. C.; Sampath, S.; Late, D. J.; Barnes, J. C.; Kleinman, S. L.; Valley, N.; Hartlieb, K. J.; Liu, Z.; Dravid, V. P.; Schatz, G. C.; Van Duyne, R. P.; Stoddart, J. F. A Semiconducting Organic Radical Cationic Host−Guest Complex. *ACS Nano* **2012**, *6*, 9964−9971. (b) Barnes, J. C.; Fahrenbach, A. C.; Cao, D.; Dyar, S. M.; Frasconi, M.; Giesener, M. A.; Benítez, D.; Tkatchouk, E.; Chernyashevskyy, O.; Shin, W. H.; Li, H.; Sampath, S.; Stern, C. L.; Sarjeant, A. A.; Hartlieb, K. J.; Liu, Z.; Carmieli, R.; Botros, Y. Y.; Choi, J. W.; Slawin, A. M. Z.; Ketterson, J. B.; Wasielewski, M. R.; Goddard, W. A.; Stoddart, J. F. A Radically Configurable Six-State Compound. *Science* **2013**, *339*, 429−433. (c) Buck, A. T.; Paletta, J. T.; Khindurangala, S. A.; Beck, C. L.; Winter, A. H. A Noncovalently Reversible Paramagnetic Switch in Water. *J. Am. Chem. Soc.* **2013**, *135*, 10594−10597. (d) Lipke, M. C.; Wu, Y.; Roy, I.; Wang, Y.; Wasielewski, M. R.; Stoddart, J. F. Shuttling Rates, Electronic States, and Hysteresis in a Ring-in-Ring Rotaxane. *ACS Cent. Sci.* **2018**, *4*, 362−371. (e) Feng, L.; Qiu, Y.; Guo, Q.-H.; Chen, Z.; Seale, J. S. W.; He, K.; Wu, H.; Feng, Y.; Farha, O. K.; Astumian, R. D.; Stoddart, J. F. Active Mechanisorption Driven by Pumping Cassettes. *Science* **2021**, *374*, 1215−1221. (f) Palmquist, M. S.; Gruschka, M. C.; Dorsainvil, J. M.; Delawder, A. O.; Saak, T. M.; Danielson, M. K.; Barnes, J. C. Electrostatic Loading and Photoredox-Based Release of Molecular Cargo from Oligoviologen-Crosslinked Microparticles. *Polym. Chem.* **2022**, *13*, 2115−2122. (g) Greene, A. F.; Danielson, M. K.; Delawder, A. O.; Liles, K. P.; Li, X.; Natraj, A.; Wellen, A.; Barnes, J. C. Redox-Responsive Artificial Molecular Muscles: Reversible Radical-Based Self-Assembly for Actuating Hydrogels. *Chem. Mater.* **2017**, *29*, 9498−9508.
(24) Constable, E. C.; Housecroft, C. E.; Kulke, T.; Lazzarini, C.; Schofield, E. R.; Zimmermann, Y. Redistribution of Terpy Ligands—Approaches to New Dynamic Combinatorial Libraries. *J. Chem. Soc. Dalton Trans.* **2001**, 2864−2871.
(25) Constable, E. C.; Housecroft, C. E.; Neuburger, M.; Phillips, D.; Raithby, P. R.; Schofield, E.; Sparr, E.; Tocher, D. A.; Zehnder, M.; Zimmermann, Y. Development of Supramolecular Structure through Alkylation of Pendant Pyridyl Functionality. *J. Chem. Soc. Dalton Trans.* **2000**, 2219−2228.
(26) (a) Aroua, S.; Todorova, T. K.; Hommes, P.; Chamoreau, L.-M.; Reissig, H.-U.; Mougel, V.; Fontecave, M. Synthesis, Characterization, and DFT Analysis of Bis-Terpyridyl-Based Molecular Cobalt Complexes. *Inorg. Chem.* **2017**, *56*, 5930−5940. (b) Yarranton, J. T.; McCusker, J. K. Ligand-Field Spectroscopy of Co(III) Complexes and the Development of a Spectrochemical Series for Low-Spin d^6 Charge-Transfer Chromophores. *J. Am. Chem. Soc.* **2022**, *144*, 12488−12500.
(27) Others have reported a related concept of tuning electronic coupling via geometric control of the spin-states of a metal: (a) Blanchard, S.; Neese, F.; Bothe, E.; Bill, E.; Weyhermüller, T.; Wieghardt, K. Square Planar vs Tetrahedral Coordination in Diamagnetic Complexes of Nickel(II) Containing Two Bidentate π-Radical Monoanions. *Inorg. Chem.* **2005**, *44*, 3636−3656. (b) Suhr, S.; Schröter, N.; Kleoff, M.; Neuman, N.; Hunger, D.; Walter, R.; Lücke, C.; Stein, F.; Demeshko, S.; Liu, H.; Reissig, H.-U.; van Slageren, J.; Sarkar, B. Spin State in Homoleptic Iron(II) Terpyridine Complexes Influences Mixed Valency and Electrocatalytic CO_2 Reduction. *Inorg. Chem.* **2023**, *62*, 6375−6386.

https://doi.org/10.1021/jacs.3c03725
J. Am. Chem. Soc. 2023, 145, 15924−15935

(28) Hanan, G.; Wang, J. A Facile Route to Sterically Hindered and Non-Hindered 4′-Aryl-2,2′:6′,2″-Terpyridines. *Synlett* **2005**, *2005*, 1251−1254.
(29) Kobayashi, M.; Masaoka, S.; Sakai, K. Synthesis, Crystal Structure, Spectroscopic and Electrochemical Properties, and H_2-Evolving Activity of a New $[PtCl(Terpyridine)]^+$ Derivative with Viologen-like Redox Properties. *Dalton Trans.* **2012**, *41*, 4903−4911.
(30) (a) Evans, C. E. B.; Naklicki, M. L.; Rezvani, A. R.; White, C. A.; Kondratiev, V. V.; Crutchley, R. J. An Investigation of Superexchange in Dinuclear Mixed-Valence Ruthenium Complexes. *J. Am. Chem. Soc.* **1998**, *120*, 13096−13103. (b) Crutchley, R. J. Intervalence Charge Transfer and Electron Exchange Studies of Dinuclear Ruthenium Complexes. In *Advances in Inorganic Chemistry*; Sykes, A. G., Ed.; Academic Press, 1994; Vol. *41*, pp 273−325.
(31) (a) Tanaka, M.; Kariya, N.; Abe, M.; Sasaki, Y. Remarkable Stabilization of a Ligand-Based Mixed-Valence State in the Metal-Based Mixed Valent $Ru_2^{II,III}$ M^{II} (μ_3-O) (M = Co, Ni) Trinuclear Cluster Complexes. *Bull. Chem. Soc. Jpn.* **2007**, *80*, 192−194. (b) Abe, M.; Sasaki, Y.; Yamada, Y.; Tsukahara, K.; Yano, S.; Yamaguchi, T.; Tominaga, M.; Taniguchi, I.; Ito, T. Oxo-Centered Mixed-Ligand Triruthenium Complexes Having Redox-Active N-Methyl-4,4′-Bipyridinium Ions ($Mbpy^+$). Reversible Multistep Electrochemical Properties of $[Ru^{III}_2Ru^{II}(M_3\text{-}O)(\mu\text{-}CH_3CO_2)_6(Mbpy^+)_2(CO)]^{2+}$ and $[Ru^{III}_3(M_3\text{-}O)(\mu\text{-}CH_3CO_2)_6(Mbpy^+)_2(L)]^{3+}$ (L = H_2O and N-Heterocyclic Ligands). *Inorg. Chem.* **1996**, *35*, 6724−6734.
(32) Viologens exhibit pyramidalization of the nitrogen atoms in their most reduced state (ref 33a 33b,), which might lead to greater ligand-centered vs metal-centered reduction in the most reduced states of $[1_x\text{-}Co]^{n+}$, lowering the influence of ancillary ligands on the n = 1+/0 redox couple.
(33) (a) Frasconi, M.; Fernando, I. R.; Wu, Y.; Liu, Z.; Liu, W.-G.; Dyar, S. M.; Barin, G.; Wasielewski, M. R.; Goddard, W. A. I.; Stoddart, J. F. Redox Control of the Binding Modes of an Organic Receptor. *J. Am. Chem. Soc.* **2015**, *137*, 11057−11068. (b) Porter, W. W.; Vaid, T. P.; Rheingold, A. L. Synthesis and Characterization of a Highly Reducing Neutral "Extended Viologen" and the Isostructural Hydrocarbon 4,4‘ “ ‘-Di-n-Octyl-p-Quaterphenyl. *J. Am. Chem. Soc.* **2005**, *127*, 16559−16566.
(34) The 3d orbitals that can couple the viologen π systems are of e symmetry in the S_4 point group of $[1_X\text{-}Co]^{n+}$ and $[2\text{-}Co]^{n+}$.
(35) As detailed in the Supporting Information, DFT methods that have been used for other MV systems (see refs 10a 10b, 11b 14a 14b 15c;) do a poor job of modeling electronic coupling in the $[1_X\text{-}Co]^{3+}$ series, producing descriptions in which all derivatives are either fully localized or fully delocalized. However, calculated energies of metal-ligand antiferromagnetic coupling correlate well with the experimental log K_c values for $[1_X\text{-}Co]^{3+}$, supporting the role of this electronic interactions in promoting delocalization.
(36) D'Alessandro, D. M.; Keene, F. R. A Cautionary Warning on the Use of Electrochemical Measurements to Calculate Comproportionation Constants for Mixed-Valence Compounds. *Dalton Trans.* **2004**, 3950−3954.
(37) Conflicting data is often seen for borderline Class II/III coupling. The $\Delta\nu_{1/2}$ values of the IVCT bands of $[1_H\text{-}Co]^{3+}$ and $[1_{Cl}\text{-}Co]^{3+}$ suggest Class IIB descriptions (ref 3a), but assignments as borderline Class II/III or Class III are supported by the experimental structure (ref 6a) and lack of solvatochromism in $[1_H\text{-}Co]^{3+}$.
(38) (a) D'Alessandro, D. M.; Keene, F. R. Intervalence Charge Transfer (IVCT) in Trinuclear and Tetranuclear Complexes of Iron, Ruthenium, and Osmium. *Chem. Rev.* **2006**, *106*, 2270−2298. (b) Chen, P.; Meyer, T. Medium Effects on Charge Transfer in Metal Complexes. *Chem. Rev.* **1998**, *98*, 1439−1478.
(39) (a) England, J.; Bill, E.; Weyhermüller, T.; Neese, F.; Atanasov, M.; Wieghardt, K. Molecular and Electronic Structures of Homoleptic Six-Coordinate Cobalt(I) Complexes of 2,2′:6′,2″-Terpyridine, 2,2′-Bipyridine, and 1,10-Phenanthroline. An Experimental and Computational Study. *Inorg. Chem.* **2015**, *54*, 12002−12018. (b) Wang, M.; Römelt, C.; Weyhermüller, T.; Wieghardt, K. Coordination Modes, Oxidation, and Protonation Levels of 2,6-Pyridinediimine and 2,2′:6′,2′′-Terpyridine Ligands in New Complexes of Cobalt, Zirconium, and Ruthenium. An Experimental and Density Functional Theory Computational Study. *Inorg. Chem.* **2019**, *58*, 121−132. (c) Scarborough, C. C.; Lancaster, K. M.; DeBeer, S.; Weyhermüller, T.; Sproules, S.; Wieghardt, K. Experimental Fingerprints for Redox-Active Terpyridine in $[Cr(tpy)_2](PF_6)n$ (n = 3−0), and the Remarkable Electronic Structure of $[Cr(tpy)_2]^{1-}$. *Inorg. Chem.* **2012**, *51*, 3718−3732.
(40) Juneau, A.; Frenette, M. Exploring Curious Covalent Bonding: Raman Identification and Thermodynamics of Perpendicular and Parallel Pancake Bonding (Pimers) of Ethyl Viologen Radical Cation Dimers. *J. Phys. Chem. B* **2021**, *125*, 10805−10812.
(41) Orbital descriptions for through-space coupling are the same for mixed-valence and homovalent pimerization: (a) Garcia-Yoldi, I.; Miller, J. S.; Novoa, J. J. Theoretical Study of the Electronic Structure of $[Tetrathiafulvalene]_2^{2+}$ Dimers and Their Long, Intradimer Multicenter Bonding in Solution and the Solid State. *J. Phys. Chem. A* **2009**, *113*, 484−492. (b) Rosokha, S. V.; Kochi, J. K. Molecular and Electronic Structures of the Long-Bonded π-Dimers of Tetrathiafulvalene Cation-Radical in Intermolecular Electron Transfer and in (Solid-State) Conductivity. *J. Am. Chem. Soc.* **2007**, *129*, 828−838. (c) Kochi, J. K.; Rathore, R.; Maguères, P. L. Stable Dimeric Aromatic Cation−Radicals. Structural and Spectral Characterization of Through-Space Charge Delocalization. *J. Org. Chem.* **2000**, *65*, 6826−6836.
(42) Mixed-valence pimerization has been enforced in supramolecular metallamacrocycles featuring related 4,4'-bipyryidine ligands: (a) Dinolfo, P. H.; Williams, M. E.; Stern, C. L.; Hupp, J. T. Rhenium-Based Molecular Rectangles as Frameworks for Ligand-Centered Mixed Valency and Optical Electron Transfer. *J. Am. Chem. Soc.* **2004**, *126*, 12989−13001. (b) Dinolfo, P. H.; Hupp, J. T. Tetra-Rhenium Molecular Rectangles as Organizational Motifs for the Investigation of Ligand-Centered Mixed Valency: Three Examples of Full Delocalization. *J. Am. Chem. Soc.* **2004**, *126*, 16814−16819.
(43) Crystals featuring other types of strong non-covalent interactions exhibit elastic flexibility: (a) Ghosh, S.; Reddy, C. M. Elastic and Bendable Caffeine Cocrystals: Implications for the Design of Flexible Organic Materials. *Angew. Chem., Int. Ed.* **2012**, *51*, 10319−10323. (b) Ghosh, S.; Mishra, M. K.; Kadambi, S. B.; Ramamurty, U.; Desiraju, G. R. Designing Elastic Organic Crystals: Highly Flexible Polyhalogenated N-Benzylideneanilines. *Angew. Chem., Int. Ed.* **2015**, *54*, 2674−2678.
(44) Similar patterns of alternating strong radical pairing and weaker van der Waals interactions have been observed in supramolecular ring-in-ring assemblies: (a) Lipke, M. C.; Cheng, T.; Wu, Y.; Arslan, H.; Xiao, H.; Wasielewski, M. R.; Goddard, W. A. I.; Stoddart, J. F. Size-Matched Radical Multivalency. *J. Am. Chem. Soc.* **2017**, *139*, 3986−3998. (b) Cai, K.; Lipke, M. C.; Liu, Z.; Nelson, J.; Cheng, T.; Shi, Y.; Cheng, C.; Shen, D.; Han, J.-M.; Vemuri, S.; Feng, Y.; Stern, C. L.; Goddard, W. A.; Wasielewski, M. R.; Stoddart, J. F. Molecular Russian Dolls. *Nat. Commun.* **2018**, *9*, 5275.
(45) (a) Han, F. S.; Higuchi, M.; Kurth, D. G. Metallosupramolecular Polyelectrolytes Self-Assembled from Various Pyridine Ring-Substituted Bisterpyridines and Metal Ions: Photophysical, Electrochemical, and Electrochromic Properties. *J. Am. Chem. Soc.* **2008**, *130*, 2073−2081. (b) Wang, C.; Hao, X.-Q.; Wang, M.; Guo, C.; Xu, B.; Tan, E. N.; Zhang, Y.-Y.; Yu, Y.; Li, Z.-Y.; Yang, H.-B.; Song, M.-P.; Li, X. Self-assembly of giant supramolecular cubes with terpyridine ligands as vertices and metals on edges. *Chem. Sci.* **2014**, *5*, 1221−1226. (c) Liu, D.; Li, K.; Chen, M.; Zhang, T.; Li, Z.; Yin, J. F.; He, L.; Wang, J.; Yin, P.; Chan, Y. T.; et al. Russian-Doll-Like Molecular Cubes. *J. Am. Chem. Soc.* **2021**, *143*, 2537−2544.

https://doi.org/10.1021/jacs.3c03725
J. Am. Chem. Soc. 2023, 145, 15924−15935